

1

# NOvA Test Beam detector calibration

2

## Technical Note

3

Róbert Králik

University of Sussex

4

October 2, 2023

5

### Abstract

6

The NOvA Test Beam detector calibration uses the same calibration procedure as the  
7 standard NOvA detectors. The main aim is to remove differences in energy deposition  
8 within the detector and to provide an absolute energy scale from collected charge to phys-  
9 ical energy units. This allows for a direct comparison of the deposited energy in the Test  
10 Beam detector with the standard NOvA detectors. On top of that, the unique qualities of  
11 Test Beam allow us to use the Test Beam calibration to validate the calibration process and  
12 possibly to provide a simulation-independent absolute energy scale.

# **13 Contents**

|   |           |
|---|-----------|
| <b>14 1 Introduction</b>                          | <b>3</b>  |
| <b>15 2 Overview of the Test Beam detector</b>    | <b>3</b>  |
| <b>16 3 NOvA calibration process</b>              | <b>7</b>  |
| 3.1 Relative calibration . . . . .                | 12        |
| 3.2 Absolute calibration . . . . .                | 13        |
| 3.3 Calibration uncertainties . . . . .           | 13        |
| <b>20 4 NOvA Test Beam detector calibration</b>   | <b>14</b> |
| 4.1 Fibre Brightness . . . . .                    | 15        |
| 4.2 Simulation . . . . .                          | 15        |
| 4.3 Threshold and shielding corrections . . . . . | 16        |
| 4.4 Period 1 . . . . .                            | 16        |
| 4.5 Period 2 . . . . .                            | 20        |
| 4.6 Period 3 . . . . .                            | 26        |
| 4.7 Period 4 . . . . .                            | 32        |
| 4.8 Absolute calibration results . . . . .        | 36        |
| 4.9 Results . . . . .                             | 36        |
| 4.10 Validation . . . . .                         | 36        |
| <b>31 5 Conclusion</b>                            | <b>51</b> |
| <b>32 References</b>                              | <b>51</b> |

## 33 1 Introduction

34 The NOvA Test Beam experiment aims to improve NOvA's sensitivity to the neutrino oscillation  
35 parameters by improving our understanding of particle interactions and energy deposition  
36 in the NOvA detectors, with the hope of reducing the total systematic uncertainty by about 10%  
37 [1].

38 Specifically, Test Beam allows us to study the response of tagged single particles as a function  
39 of their measured energies and compare it to the simulated prediction. It also enables us to  
40 determine the energy resolution and the absolute energy scale of these particles. Additionally,  
41 we are able to compare the response of beam and cosmic ray muons, to study fibre attenuation,  
42 or to validate the entire NOvA calibration process. Test Beam detector was also equipped with  
43 a combination of near and far detector readout electronics and filled with a variety of NOvA  
44 scintillator oils, which makes it possible to make a comparison of their responses [2].

45 All the aforementioned benefits of running the NOvA Test Beam experiment require, or  
46 benefit from, the Test Beam detector calibration.

47 The Test Beam detector calibration was first pioneered by Kevin Moulder who adapted the  
48 NOvA calibration codebase for Test Beam and tested it on period 1 Test Beam data [3]. This  
49 was followed by Anna Hall who improved it and got the first usable calibration of the Test  
50 Beam detector based on the period 2 data [4]. Lastly, Rober Kralik took over and finished the  
51 Test Beam calibration with all Test Beam data and a new simulation in 2023 [5].

## 52 2 Overview of the Test Beam detector

53 The NOvA Test Beam detector is a scaled down version of the near and far detectors shown on  
54 figure 1. It is placed in the MC7b enclosure of the Fermilab Test Beam Facility in the path of  
55 the MCcenter beamline with a variety of beamline detectors to measure and identify a range of  
56 particles with various momenta [6].

57 The Test Beam detector started with commissioning runs in May 2019 and ran, with an  
58 exception of regular summer shutdowns, until July 2022, after which it was decommissioned.  
The Test Beam data periods are:

|          |                                |                               |
|----------|--------------------------------|-------------------------------|
| Period 1 | March 22 <sup>nd</sup> 2019    | - July 6 <sup>th</sup> 2019   |
| Period 2 | December 5 <sup>th</sup> 2019  | - March 20 <sup>th</sup> 2020 |
| Period 3 | January 12 <sup>th</sup> 2021  | - June 27 <sup>th</sup> 2021  |
| Period 4 | November 30 <sup>th</sup> 2021 | - July 10 <sup>th</sup> 2022  |

Table 1: Test Beam detector data taking periods.

59  
60 Majority of the Test Beam detector and its instrumentation is identical to the other NOvA  
61 detectors, with a few exceptions that could have an impact on the calibration. We are going to  
62 identify and discuss these differences in this section.

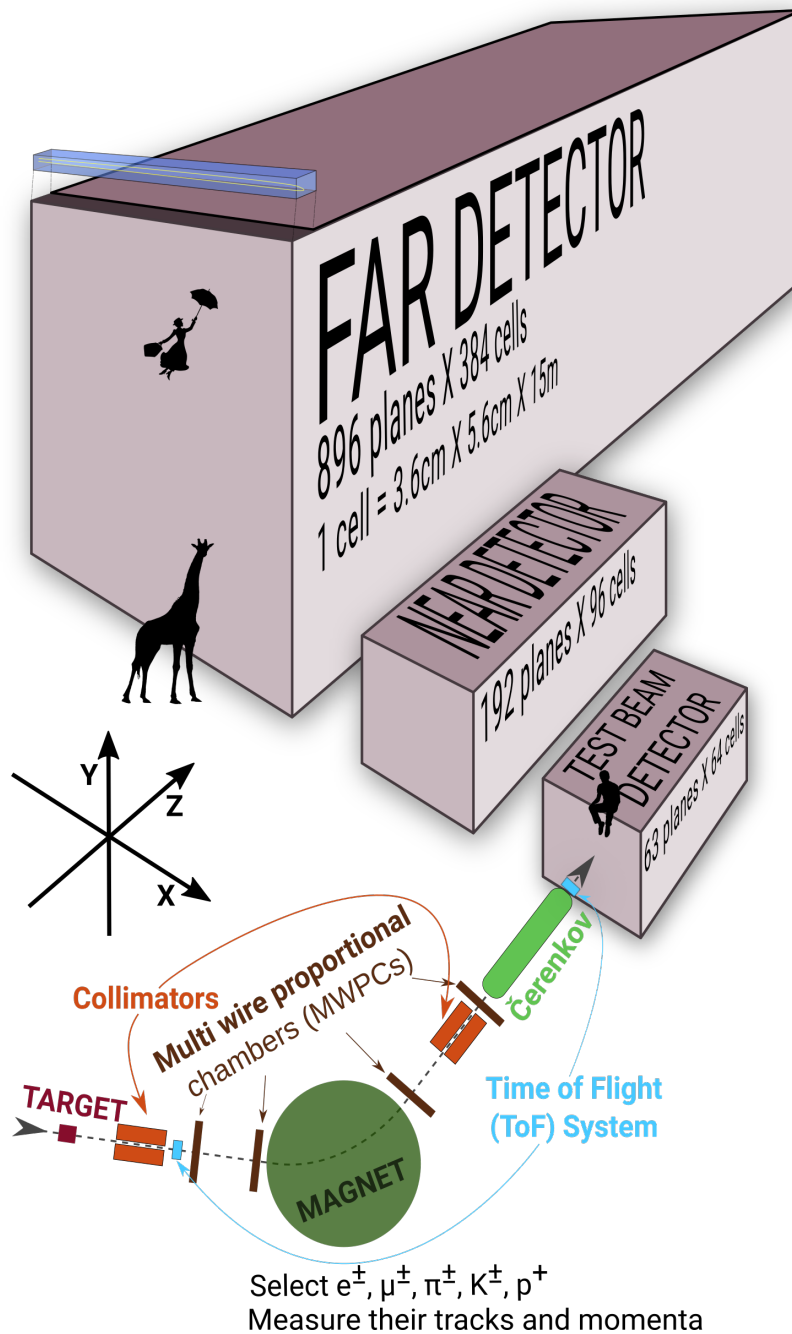


Figure 1: Comparison of Test Beam detector scale to the Near and Far NOvA detectors (and a man, giraffe, or Mary Poppins). Also shown are the Test Beam beamline detectors and components (not to scale), with arrows showing the direction of the beam. The three black arrows show the orientation of the detector coordinate system.

### 63 General parameters

- 64 The NOvA Test Beam detector consists of two 31-plane blocks, each beginning and ending  
 65 with a vertical plane, with an additional horizontal plane glued in-between them to preserve  
 66 the alternating pattern [7]. Each plane consists of 2 modules side-by-side, both made up of 32

67 cells. Each cell is 2.6 m long with an inner (without the PVC) depth and width of 5.9 cm and  
68 3.8 cm respectively, same as for the other NOvA detectors. This brings the final dimensions of  
69 the Test Beam detector to 63 planes  $\times$  64 cells, or  $2.6 \times 2.6 \times 4.1 \text{ m}^3$ .

70 The 63 planes are numbered from 0 to 62, with even numbers corresponding to vertical  
71 planes and odd numbers to horizontal planes. Cells are numbered 0 to 63, going from bottom  
72 to top for horizontal planes and left to right, when facing the front of the detector, for vertical  
73 planes.

74 The detector coordinate system is illustrated on figure 1. It is centred with (0,0,0) in the  
75 centre of the first plane [8]. The x axis runs left to right when facing the front of the detector,  
76 y axis bottom to top, and z axis goes along the beam direction from front to the back of the  
77 detector. Position within each cell ( $w$ ) is aligned with the x (y) axis for the horizontal (vertical)  
78 cells, with  $w = 0$  centred in the middle of each cell. The exact geometry of the Test Beam  
79 detector was measured in several alignment surveys and is saved in gdml files [9].

80 In the past we encountered an issue when trying to align the Test Beam detector with the  
81 beamline measurements by rotating the detector. This broke several assumptions within the  
82 Test Beam geometry [8] and manifested as uncalibrated cells in the back of the detector [10].  
83 This was fixed by realigning both the detector and the beamline separately, based on the last  
84 alignment survey, measured during the decommissioning of the detector. We implemented the  
85 fix in the production tag R23-04-05-testbeam-production.a [8].

## 86 Scintillator

87 Test Beam used a combination of the leftover near and far detector production scintillator oils  
88 and the oil drained from the NDOS test detector. The used scintillator oils also differ in the  
89 way they were stored since the filling of the near and far detectors, or NDOS draining, which  
90 apparently impacted its quality. The distribution of individual scintillator oils and the relative  
91 difference in their energy response can be seen on figure 2.

92 We can distinguish four samples of the NOvA scintillator oil used in the Test Beam detector:

- 93 • Mixed near detector production oil and NDOS-drained oil stored in a tanker and tanks  
94 outside in Fermilab [11];
- 95 • Separate near detector production oil and NDOS-drained oil stored underground in barrels  
96 at MiniBooNE [1];
- 97 • Far detector production oil stored inside in Ash River in "totes" under several layers of  
98 black plastic [12];
- 99 • NDOS-drained oil stored mainly inside at Texas A&M University and University of  
100 Texas at Austin [13, 14].

101 The original plan [15] was to only use the tanker/tank scintillator (sample 1). First tests  
102 showed acceptable results and the tanker oil was used to fill out almost the entirety of the first  
103 block of the detector (first 32 planes) [11]. However, when we loaded oil from tank two into  
104 the tanker, it became extremely cloudy and unusable, possibly due to contamination with water  
105 accumulated at the bottom of the tanks. The rest of the first block was therefore topped up with  
106 high quality scintillator from NDOS (sample 2). This is labelled as "Fermilab ND+NDOS oil"  
107 on figure 2.

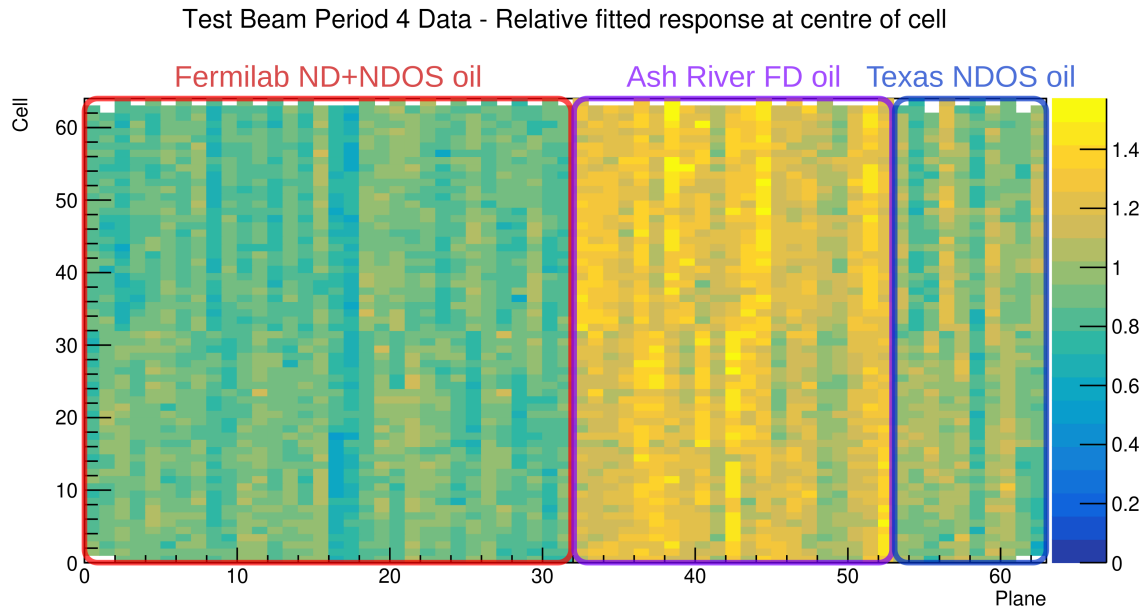


Figure 2: Uncorrected energy response in the centre of cells across the Test Beam detector showing a clear distinction between the different scintillator oils, shown with coloured boxes.

108     The first 21 planes of the second block (planes 32 to 52) were filled with the far detector  
 109    production scintillator shipped in from Ash River (sample 3) [16]. We again topped up these  
 110    planes with the ND+NDOS scintillator (sample 2) [16].

111     The last 10 planes (planes 53 to 62) [16] were filled with the "Texas" scintillator (sample  
 112    4), which has higher light yield than the one from the tanker, but lower than the Ash River one  
 113    [13].

114     In total the Test Beam detector is filled with 5418 gallons of scintillator oil with a weight  
 115    of approximately 28.6 tons [7].

### 116   **Readout**

117     The Test Beam detector uses in total 126 Front End Boards (FEBs), each reading out signal  
 118    from 32 cells (one module = half of a plane) [7]. The readout is located on the top and right  
 119    side (when looking at the front) of the detector. 118 FEBs are version 4.1, same as in the Far  
 120    Detector, and 8 FEBs, located in pairs on planes 16, 17, 48 and 49, are version 5.2, same as in  
 121    the Near Detector. The Near Detector FEBs are designed to read out data in a faster rate and we  
 122    used a mix of FEB types to study the difference in their response and to validate both versions  
 123    in the same environment [17].

### 124   **Environment**

125     Unlike the near and the far detector, the Test Beam detector does not have any overburden to  
 126    shield it from cosmic particles, which affects their rate and energies inside the detector. There  
 127    is also less precise control of temperature and humidity than in the other detectors [source?],  
 128    which can potentially impact the scintillator and readout performance.

129 **Underfilled cells issue**

130 The Test Beam detector is slightly tilted around the Z axis by about  $0.7^\circ$  towards the readout.  
131 This caused the top cells of both modules of all the horizontal planes (cells 31 and 63) to be  
132 underfilled, creating an air bubble on the left side of the detector and severely affecting the  
133 energy response in those cells [17]. This has been fixed [18] during the period 3 running by  
134 adding extensions to the filling ports and overfilling the horizontal cells with the ND+NDOS  
135 scintillator (sample 2).

136 **3 NOvA calibration process**

137 Test Beam is following the same ideas and procedures as the standard NOvA calibration. This  
138 section intends to provide only a brief overview of the NOvA calibration, with further details  
139 in the range of NOvA calibration technical notes [19]. All the code required for calibration is  
140 located in the NOvASoft Calibration package and the outline of the files and processes in  
141 NOvA calibration are shown on figure 3.

142 The purpose of calibration is to make sure that we get the same amount of energy wherever  
143 or whenever it's deposited in whichever of NOvA's detectors and to express this amount of  
144 energy in physical units. The NOvA calibration uses cosmic ray muons, which provide a  
145 consistent, abundant, and well-understood source of energy deposition and consists of two  
146 parts [20]:

- 147 1. The **relative calibration** corrects for attenuation of scintillator light as it travels through  
148 the cell to the readout, as well as for differences between detector cells. This correction  
149 is calculated for each cell separately.
- 150 2. Followed by the **absolute calibration**, which only uses stopping muons when they are  
151 minimum ionising particles. In the absolute calibration we calculate a scale between  
152 the measured energy deposition, corrected by the relative calibration, and the simulated  
153 energy deposition in physical units of MeV. This scale is calculated for each time period  
154 and each detector separately, which ensures the energy deposition is directly comparable  
155 wherever or whenever it occurred.

156 The NOvA calibration process technically also involves **timing calibration**, which corrects  
157 for the time differences of the signal to be processed [21]. However, this is done as a separate  
158 project to the relative and absolute calibrations and is out of scope of this technical note.

159 The basic units and variables used to define energy deposited in the NOvA detectors are  
160 listed in table 2.

The final result of the NOvA calibration is the deposited energy in terms of physical units,

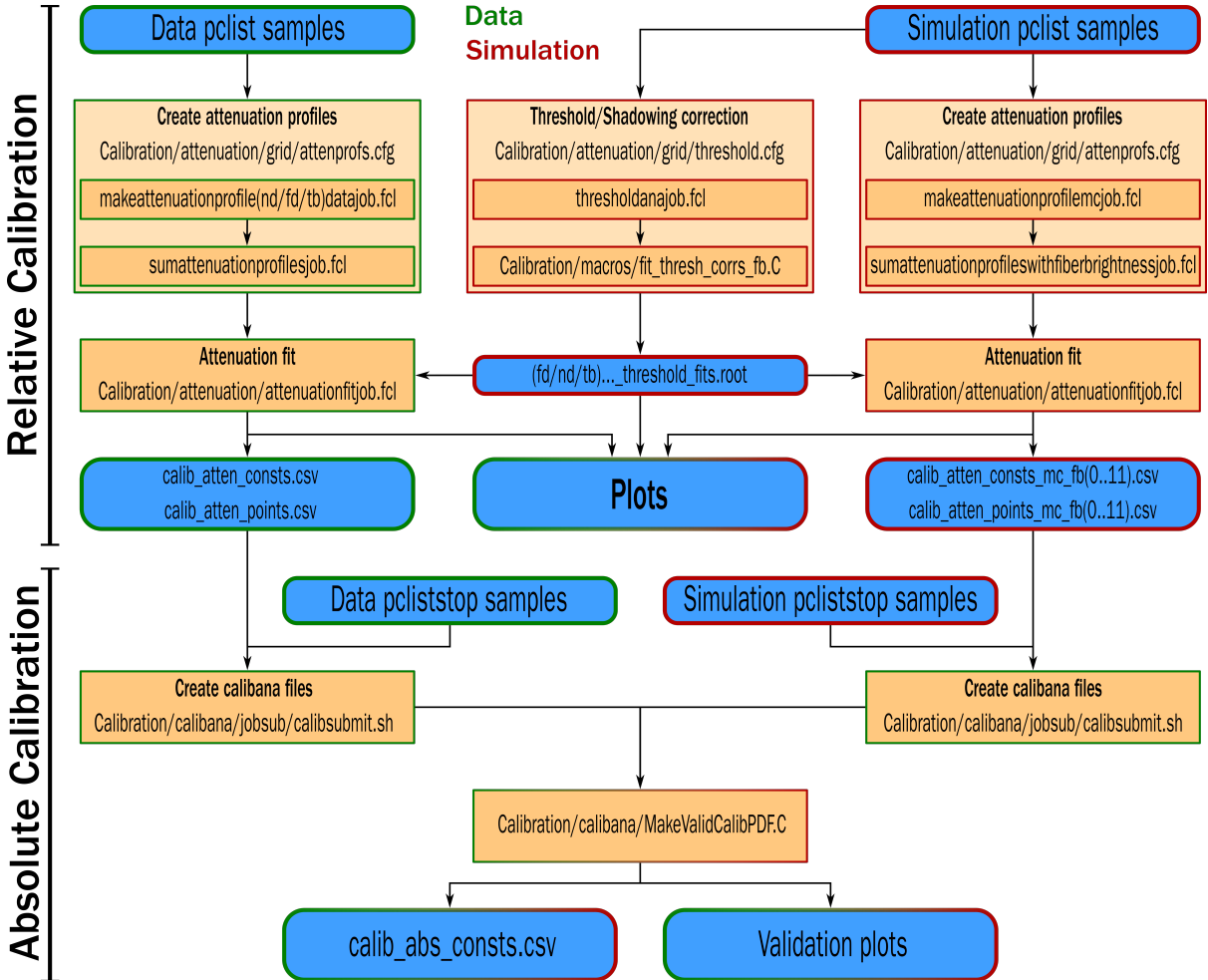


Figure 3: Flow chart showing the jobs (orange background) and files (blue background) needed and produced during the full NOvA calibration process. The left chain is showing the data calibration process (with green border) and is applied to every data calibration sample separately (periods or epochs). The center and right chains are showing the simulation calibration process (red border), which is redone only if there's a change to the detector simulation. The absolute calibration at the bottom combines data and simulation. The entire process is done separately for each NOvA detector.

|        |  |
|--------|--|
| ADC    | The digitized charge collected by the APDs from the Analog to Digital Converter [22].  |
| PE     | Number of Photo Electrons. Calculated by a simple rescaling of the best estimate of the peak ADC. The PE per ADC scale only depends on the FEB type and the APD gain settings. This conversion is done before the calibration and PE serves as the base unit for calibration.  |
| PECorr | Corrected PE after applying the relative calibration results. The correction is a ratio between an average energy response (a pre-determined semi-arbitrary number) and the result of the the relative calibration fit (also called attenuation fit), which depends on w, cell, plane, epoch and detector. This makes the energy response equivalent across each detector. |
| MEU    | Muon Energy Unit is the mean detector response to a stopping cosmic minimum ionising muon. For true variables it's equivalent to the mean MeV/cm and for reconstructed variables to the mean PECorr/cm.  |
| MeV    | Estimated energy deposited in the scintillator calculated from PECorr using the results of the absolute calibration. Additional correction for dead material needs to be made in order to get an estimate of the calorimetric energy.  |

Table 2: Definitions of variables commonly used in calibration [19, 20].

which is in effect calculated as:

$$E_{dep}[\text{MeV}] = \underbrace{\frac{\text{MEU}_{truth}[\text{MeV}/\text{cm}]}{\text{MEU}_{reco}[\text{PECorr}/\text{cm}]}}_{\substack{\text{Absolute calibration} \\ (\text{Detector, epoch})}} \times \underbrace{\frac{\text{Average response}[\text{PECorr}]}{\text{Fitted response}[\text{PE}]}}_{\substack{\text{Relative calibration} \\ (\text{Detector, epoch, plane, cell, w})}} \times \underbrace{\left[ \frac{\text{PE}}{\text{ADC}} \right]}_{\substack{\text{Scale} \\ (\text{APD Gain, FEB})}} \times \text{Signal}[\text{ADC}], \quad (1)$$

where both the relative calibration results (blue fraction) and the absolute calibration results (red fraction) are stored in a database and applied together with the ADC-to-PE scale by the NOvASoft Calibrator package during processing of every hit in the NOvA detectors.

#### Creating calibration samples

We want to select good quality cosmic ray muons. First, we remove beam related events based on their time stamps relative to the time of the beam spill, using the RemoveBeamSpills (for the near and far detectors), or RemoveTBSpills filter (for the Test Beam detector), as shown on figure 4. Next we apply reconstruction to get the CellHit, slicer, and track information, followed by a track-based selection to remove misreconstructed and poor quality events.

Since energy deposition depends on the path length particle travels through a cell, we only use hits for which we can reliably calculate their path length. We call these hits **tricell** hits, as we require that all accepted hits are accompanied by a recorded hit in both neighbouring cells of the same plane, as shown on figure 5. In case there is a bad channel in a neighbouring cell,

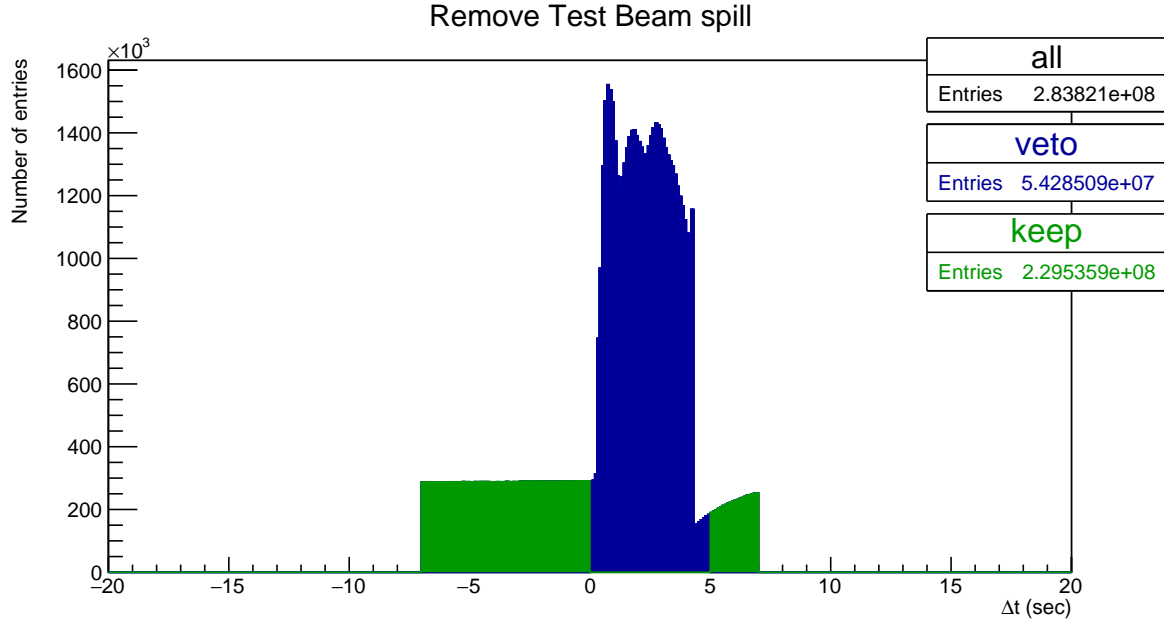


Figure 4: Test Beam beam spill events removed from the calibration samples. Test Beam beam spill is 4.2 seconds long and we remove events (in blue) within a 5 seconds window from the start of the beam spill. The remaining events (green) should mostly consist of cosmic particles. This example and the numbers of entries are for the full period 4 Test Beam sample.

<sup>174</sup> we ignore this channel and look one cell further. We can then calculate the path length simply  
<sup>175</sup> as the cell width divided by the cosine of the direction angle [19, 20].

<sup>176</sup> For the absolute calibration we select muons that stop inside the detector, by identifying  
<sup>177</sup> muons with a Michel electron at the end of their track [23].

<sup>178</sup> For each data period or epoch and for each version of the simulation we create two calibra-  
<sup>179</sup> tion samples that are used as the input for the relative and absolute calibration. The samples  
<sup>180</sup> are called [24]

- <sup>181</sup> • pclist = **list** of pre-calibrated hist; Contains all selected cosmic muon events and is used  
<sup>182</sup> in the relative calibration;
- <sup>183</sup> • pcliststop = pclist files only containing stopping muons used for the absolute calibration

#### <sup>184</sup> Fibre brightness

<sup>185</sup> For data, the relative calibration is done for each individual cell in each plane to properly  
<sup>186</sup> account for any potential variations, repeating the attenuation fit  $N_{cell} \times N_{plane}$  times. However,  
<sup>187</sup> generating enough simulated events turned out to be computationally expensive. Therefore,  
<sup>188</sup> assuming the simulated detector is approximately uniform plane to plane, for simulation we  
<sup>189</sup> can "consolidate" the detector planes and only consider variations in the two views. Therefore  
<sup>190</sup> for simulation we would repeat the fit  $N_{cell} \times N_{view}$  times [25, 26].

<sup>191</sup> However, there are some variations in the detector response cell by cell that can be caused  
<sup>192</sup> by different fibre brightnesses, but also by different qualities of the scintillator, air bubbles,  
<sup>193</sup> APD gains, looped or zipped fibres and potentially others. We want to include these variations

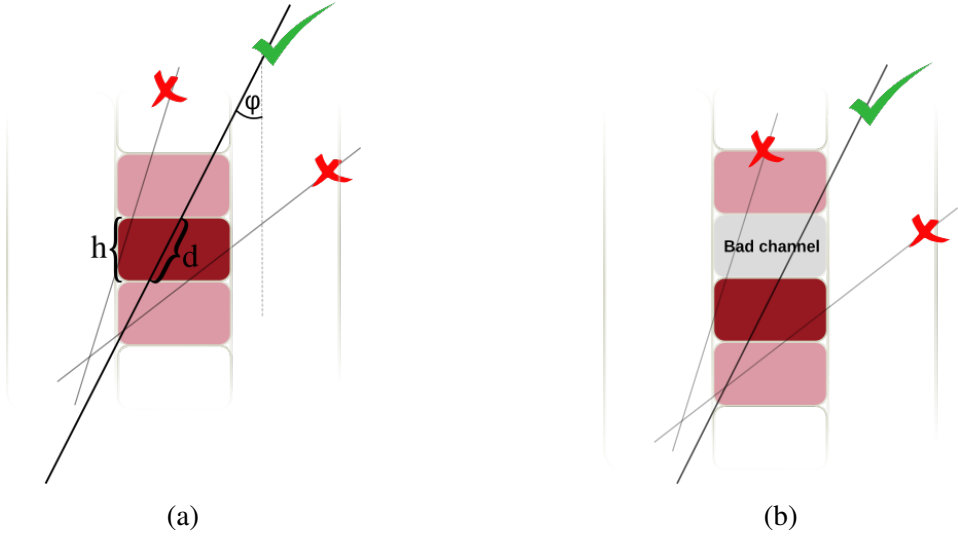


Figure 5: Illustration of the tricell condition (a). We only use hits that have two surrounding hits in the same plane to be used in the NOvA calibration. This is to ensure a good quality of the path length ( $d$ ) reconstruction, which is calculated from the known cell height ( $h$ ) and the reconstructed track angle ( $\phi$ ). In case the hit is next to a bad channel (b), we ignore this bad channel and require a hit in the next cell over.

in the simulation to better match data. To emulate these differences in the simulation without the need to simulate every cell individually, we divide each detector into 12 brightness bins, as shown on figure 6. These brightness bins describe the relative differences in the detector response between individual cells [26]. Therefore in the end, for simulation we perform the attenuation fit  $N_{cell} \times N_{view} \times N_{BrightnessBin}$  times.

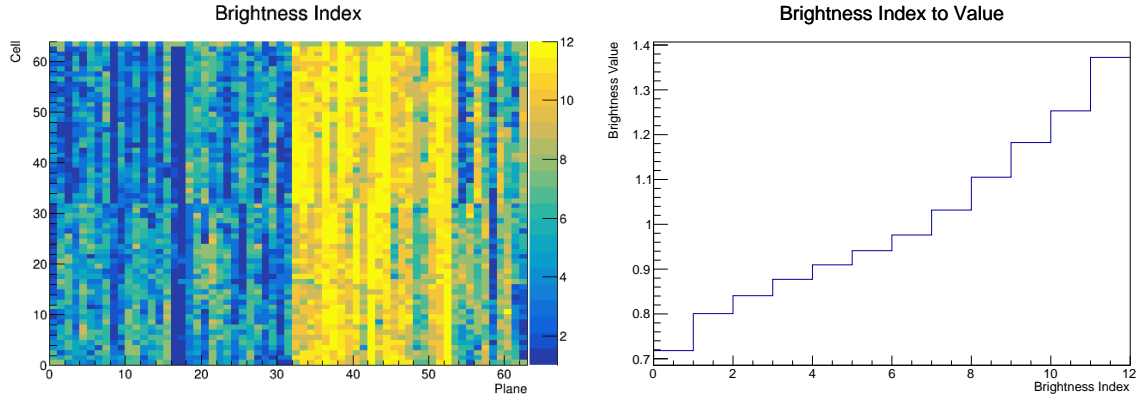


Figure 6: The Test Beam detector is (like the standard NOvA detectors) divided into 12 brightness bins (left plot), each representing a relative difference in energy response (right plot) due to different brightnesses of the fibres, scintillators, or readout.

To divide each detector into the 12 brightness bins, we use results from the relative calibration. Specifically we take the result of the attenuation fit (equal to the average response) in the centre of each cell and fill a 2D histogram. Then we normalize this response by dividing the response in each Cell  $\times$  View  $\times$  Plane by the average response in the corresponding

203 Cell  $\times$  View. Then we make a 1D histogram filled with the normalized responses of each cell  
204 and divide this histogram into 12 equally populated bins (so each bin represents approximately  
205 the same number of detector cells, shown on the left plot of figure 6). The mean normalized  
206 response in each bin represents the relative brightness value of this bin (right plot of figure  
207 6). A ROOT file with the distribution of brightness bins across the detector and their corre-  
208 sponding relative brightness values is stored inside the NOvAsoft PhotonTransport package  
209 as <det>BrightnessFromCosmics.root.

210 **Threshold and shielding correction**

211 Energy deposited far away from the readout may get attenuated enough to be shifted below the  
212 threshold. These low energy depositions would be missing from the attenuation fit, biasing it  
213 towards larger light levels with increasing distance from the readout. Similar effect, specifically  
214 for the vertical cells, is caused by using cosmic muons for calibration and applying it to beam  
215 muons. The top of the detector effectively shields the bottom, skewing the energy distribution  
216 of cosmic muons. To correct for both of these effect, we use the simulation plist sample to  
217 calculate the threshold and shielding (also called threshold and shadowing) correction by com-  
218 paring the true and reconstructed information. We apply this correction before the attenuation  
219 fits [25].

220 **3.1 Relative calibration**

221 Relative calibration corrects for the attenuation of the scintillator light by fitting the average  
222 detector response over the position in each cell ( $w$ ), separately for every cell inside each de-  
223 tector. Dividing the "average response" of the detector by the result of the attenuation fit for  
224 each Plane  $\times$  Cell  $\times w$  combination effectively removes relative differences within and between  
225 all cells across the entire detector. The average response is a single constant number chosen to  
226 approximately represent the average response in the middle of the cell. Its value is for the far  
227 detector and Test Beam 39.91 PE and for the near detector 37.51 PE. The value of the average  
228 response has no impact of the calibration results, as the absolute scale of the detector response  
229 is determined during the absolute calibration and relative calibration only serves to remove the  
230 relative differences [20, 25].

231 To create the attenuation fit we use the following procedure [20]:

- 232 Create the *attenuation profiles*. Attenuation profiles are essentially profile histograms of  
233 detector response in terms of PE/cm as a function of position in the cell ( $w$ ) for each cell  
234 in all planes. We construct the attenuation profiles over a little wider range than the actual  
235 length of the cell and always with 100 bins for each detector. This means that smaller  
236 detectors, like the Test Beam detector, have a finer binning ( $\sim 3\text{cm/bin}$ ) compared to the  
237 Far Detector ( $\sim 18\text{cm/bin}$ ).
- 238 Analyse the attenuation profiles. The job to create the attenuation profiles also creates  
239 validation histograms, which should be analysed prior to performing the attenuation fit  
240 to make sure the attenuation profiles look as expected.
- 241 Apply the threshold and shielding correction that was created before the relative calibra-  
242 tion.

243 4. Do the attenuation fit over the full length of each cell. The fit consists of

- (a) an exponential fit, which combines two cases. First, when the scintillating light travels the short distance straight to the readout, and second, when it goes to the far side of the cell and loops around before going to the readout. The fitted function has a form:

$$y = C + A \left( \exp\left(\frac{w}{X}\right) + \exp\left(-\frac{L+w}{X}\right) \right), \quad (2)$$

244 where  $y$  is the fitted response,  $L$  is the length of the cell and  $C$ ,  $A$  and  $X$  are the fitted 245 parameters.  $X$  also represents the attenuation length.

- 246 (b) Smoothing of the residuals from the exponential fit, mainly at the end of cells, with 247 the LOcally WEighted Scatter plot Smoothing (LOWESS) method.

248 5. Check the plots of the attenuation fit for a selection of cells.

249 6. Save the fit result to the database in the form of two csv tables. The `calib_atten_consts.csv` 250 table holds the results of the exponential fit, together with the final  $\chi^2$  of the fit. The 251 `calib_atten_points.csv` table holds the results of the LOWESS smoothing.

252 To ensure the quality of the attenuation fit, we only apply the results if the final  $\chi^2 < 0.2$ . 253 If  $\chi^2 > 0.2$ , we ignore the results for this cell and mark it as *uncalibrated*.

## 254 3.2 Absolute calibration

255 To find the absolute energy scale, we apply the relative calibration results on the stopping 256 muon sample and look at the energy they deposited in cells 1-2 meters from the end of their 257 tracks. In this track window they are approximately minimum ionising particles and their 258 energy deposition is almost constant and well understood. Additionally, we don't use hits from 259 the edges of a cell, as those might be affected by the lower number of events and fibre endings, 260 or loops. We take a mean of their corrected deposited energy separate for each view and for 261 each calibrated sample. We then take the average over the two views to get the final  $\text{MEU}_{reco}$  262 in PECorr/cm for each sample [23].

263 From simulation we get the mean of the true energy deposited in scintillator  $\text{MEU}_{truth}$  in 264 MeV/cm for the same sample of stopping muons. We ignore the energy that is lost in the 265 dead material (PVC extrusions) and deal with it separately. The absolute energy scale for each 266 sample is then the ratio of  $\text{MEU}_{truth}/\text{MEU}_{reco}$ . We save these absolute energy scales in another 267 csv table called `calib_abs_consts.csv` which stores the MEU values and their errors.

268 As part of the absolute calibration we also produce validation plots that show the effect of 269 calibration on the distribution of the stopping muons. We analyse these plots and if everything 270 looks all right we load all the csv tables into the database.

## 271 3.3 Calibration uncertainties

### 272 WORK IN PROGRESS

## <sup>273</sup> 4 NOvA Test Beam detector calibration

<sup>274</sup> In this section we describe the details of the Test Beam detector calibration as it was finalized  
<sup>275</sup> in June 2023. This version includes all measured Test Beam data, with the exception of Period  
<sup>276</sup> 1, which was only used for commissioning and is not used in any Test Beam analysis. The  
<sup>277</sup> specific commands and tips for running the Test Beam detector calibration are listed on the  
<sup>278</sup> [Test Beam calibration redmine wiki page](#).

<sup>279</sup> The calibration samples used for the Test Beam detector calibration are listed in table 3. We  
<sup>280</sup> are using data from one of the Test Beam data-driven activity-based triggers (DDActivity1). To  
<sup>281</sup> produce these samples we (or production) use the `prod_tb_ddactivity1_pclist_job.fcl` FHiCL  
<sup>282</sup> file from the novaproduct/novaproduction/fcl/testbeam repository, or the corresponding mc file.  
<sup>283</sup> The calibration samples were originally created in keep-ups by the production, but most of  
<sup>284</sup> them had to be reproduced in 2023 to fix a bug in the Test Beam geometry.

---

### pclist samples

#### **Data period 2:**

`prod_pclist_R23-04-05-testbeam-production.a_testbeam_ddactivity1_period2_v1`

#### **Data period 3:**

`prod_pclist_R23-04-05-testbeam-production.a_testbeam_ddactivity1_epoch3a_v1`

`prod_pclist_R23-04-05-testbeam-production.a_testbeam_ddactivity1_epoch3b_v1`

`prod_pclist_R23-04-05-testbeam-production.a_testbeam_ddactivity1_epoch3c_v1`

`pclist_testbeam_detector_activity_epoch3d_R21-01-28-testbeam-production.a`

`pclist_testbeam_detector_activity_epoch3e_R21-01-28-testbeam-production.a`

#### **Data period 4:**

`prod_pclist_R23-04-05-testbeam-production.a_testbeam_ddactivity1_period4_v1`

#### **Simulation:**

`rkrilik_pclist_testbeam_databasedsim_R23-04-05-testbeam-production.a`

---

### pcliststop samples

#### **Data period 2:**

`prod_pcliststop_R23-04-05-testbeam-production.a_testbeam_ddactivity1_period2_v1`

#### **Data period 3:**

`prod_pcliststop_R23-04-05-testbeam-production.a_testbeam_ddactivity1_epoch3a_v1`

`prod_pcliststop_R23-04-05-testbeam-production.a_testbeam_ddactivity1_epoch3b_v1`

`prod_pcliststop_R23-04-05-testbeam-production.a_testbeam_ddactivity1_epoch3c_v1`

`pcliststop_testbeam_detector_activity_epoch3d_R21-01-28-testbeam-production.a`

`pcliststop_testbeam_detector_activity_epoch3e_R21-01-28-testbeam-production.a`

#### **Data period 4:**

`prod_pcliststop_R23-04-05-testbeam-production.a_testbeam_ddactivity1_period4_v1`

#### **Simulation:**

`rkrilik_pcliststop_testbeam_databasedsim_R23-04-05-testbeam-production.a`

---

Table 3: SAMWEB definitions of the Test Beam calibration samples.

## 285 4.1 Fibre Brightness

286 To divide the Test Beam detector into fibre brightness bins we used the attenuation fit results  
 287 for period 4 data (described in section 4.7), since that is the best detector conditions data we  
 288 have. As we are only using the attenuation fit results in the centre of each cell, we've decided  
 289 to allow some cells that initially failed the calibration, to be still used for the creation of the  
 290 brightness file. As can be seen on figure 7, some attenuation fits have  $\chi^2 > 0.2$ , even though  
 291 they correctly represent the energy deposition in the centre of that cell. By carefully investigating  
 292 all cells with  $\chi^2 > 0.2$  (possible for Test Beam, due to its small number of cells), we concluded  
 293 it is safe to use all attenuation fit results, for which  $\chi^2 < 0.7$ .

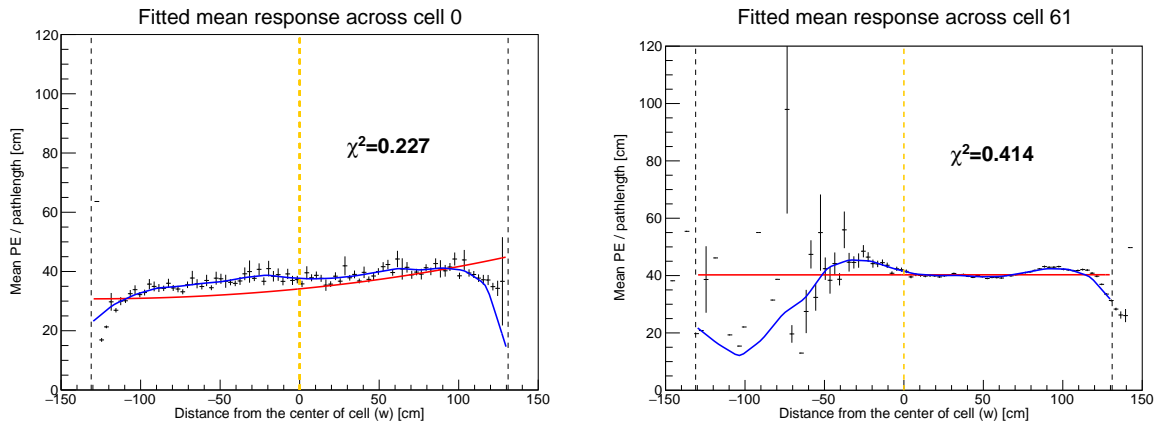


Figure 7: Attenuation fits for two cells that fail the calibration condition, but the fit (blue line) correctly represents the energy deposition in the centre of that cell (yellow dashed line).

## 294 4.2 Simulation

295 We used a data-based simulation of cosmic muons for the Test Beam detector calibration. The  
 296 details are described in the Data-based simulation of cosmic muons (not only) for calibration  
 297 technical note [27]. We used half of period 4 data (used every second event as saved in the root  
 298 file, therefore sampled from the entire period 4) as inputs and the newly created fibre brightness  
 299 file to inform the simulation on the realistic detector conditions.

300 The distribution of events cosmic muon events from the new simulation is shown on figure  
 301 8.

302 The results of the attenuation fit are shown for each cell (in its centre) on figure 9. The  
 303 blank cells show which cells failed the attenuation fit (their  $\chi^2 > 0.2$ ). Most of the uncalibrated  
 304 cells are on the edges of the detector, which is expected as those have much fewer events that  
 305 pass our selection than the rest. Examples of a standard detector response and of the response  
 306 for cells on the edge of the detector are shown of figure 10.

307 (I should explain here what is on the plots maybe - red is the exponential fit and blue is the  
 308 total with with the LOWESS. Most cells have the expected response of slow rise towards the  
 309 readout falling down on the edges).

310 There is only one cell in the middle of the detector that is left uncalibrated, which is the cell  
 311 32 in a vertical plane in the brightness bin 5, shown on the top right of fig.10. The corresponding

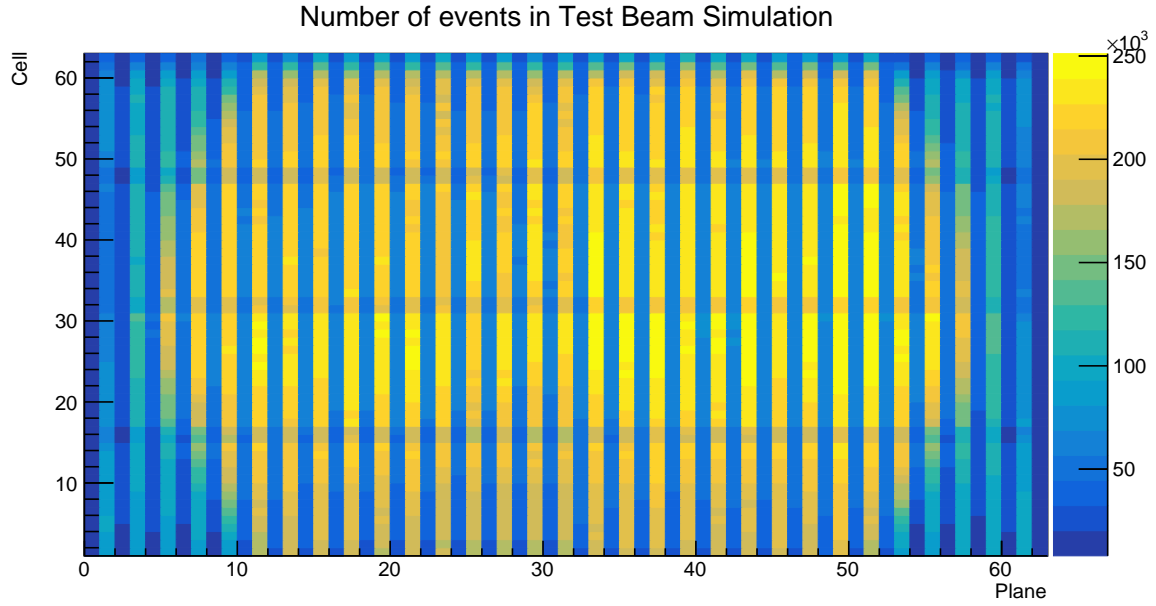


Figure 8: Distribution of events in the Test Beam simulation calibration sample.

<sub>312</sub>  $\chi^2 = 0.227$ . It seems the reason the  $\chi^2 > 0.2$  is an exceptionally high response with a large  
<sub>313</sub> uncertainty in the last bin.

<sub>314</sub> This is a much better result of the relative calibration (attenuation fit) for a simulation than  
<sub>315</sub> the previous versions of Test Beam detector calibration simulations were able to accomplish.

### <sub>316</sub> 4.3 Threshold and shielding corrections

<sub>317</sub> The threshold and shielding correction for Test Beam is almost uniform across all cells as can  
<sub>318</sub> be seen on figure 11. This is expected as the height of the Test Beam detector is 2.6 m has only  
<sub>319</sub> a negligible effect on the energy distribution of cosmic muons or on the threshold saturation.  
<sub>320</sub> The correction is basically just a normalization factor, except for the cell edges, but there is a  
<sub>321</sub> large variation in the energy response there anyway due to low number of events. Since the  
<sub>322</sub> relative calibration only cares about relative differences across the detector, a normalization  
<sub>323</sub> factor doesn't change anything.

### <sub>324</sub> 4.4 Period 1

<sub>325</sub> TO DO: add a description of period 1 data

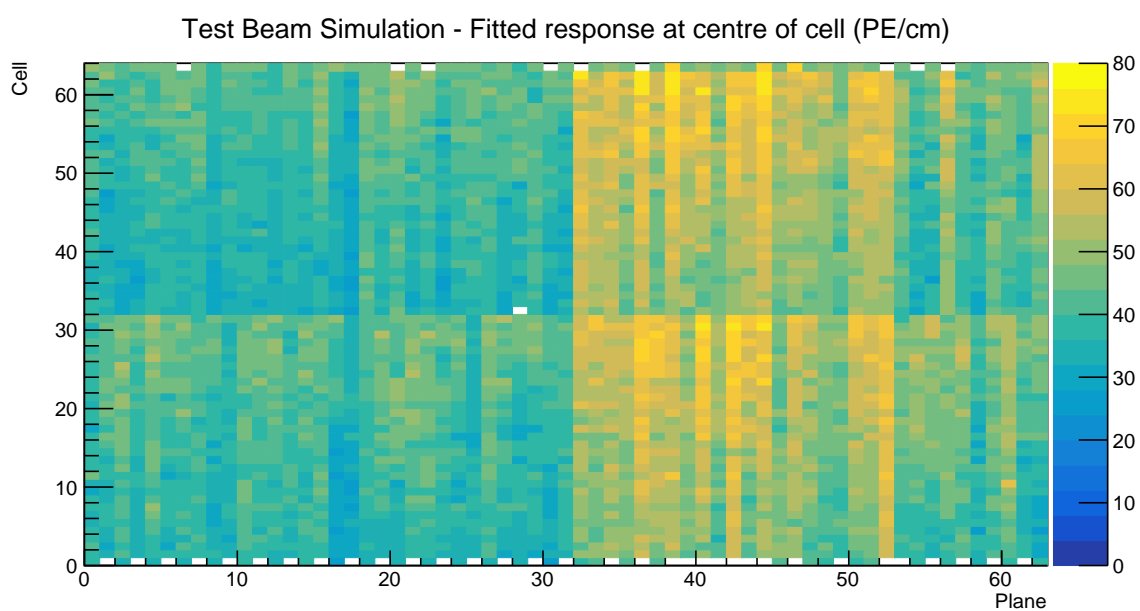


Figure 9: Overview of the attenuation fit results for the Test Beam detector calibration simulation. Each cell represents the result of the attenuation fit to the energy response in the centre of that cell. The blank cells are uncalibrated.

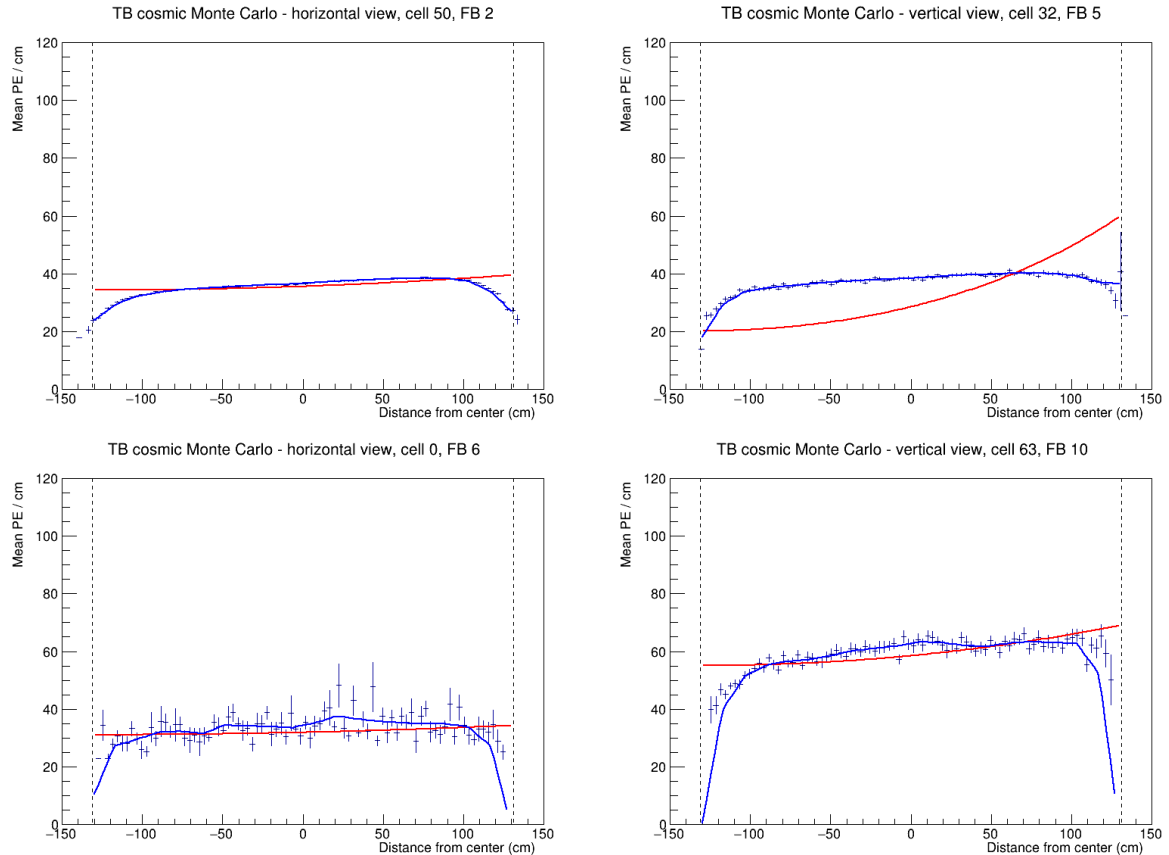


Figure 10: Attenuation fits for a selection of cells in the Test Beam calibration simulation. Top left is an example of a successful attenuation fit, top right is a failed fit due to statistical fluctuation in the last bin and the bottom plots show failed fits for cells on the edges of the detector.

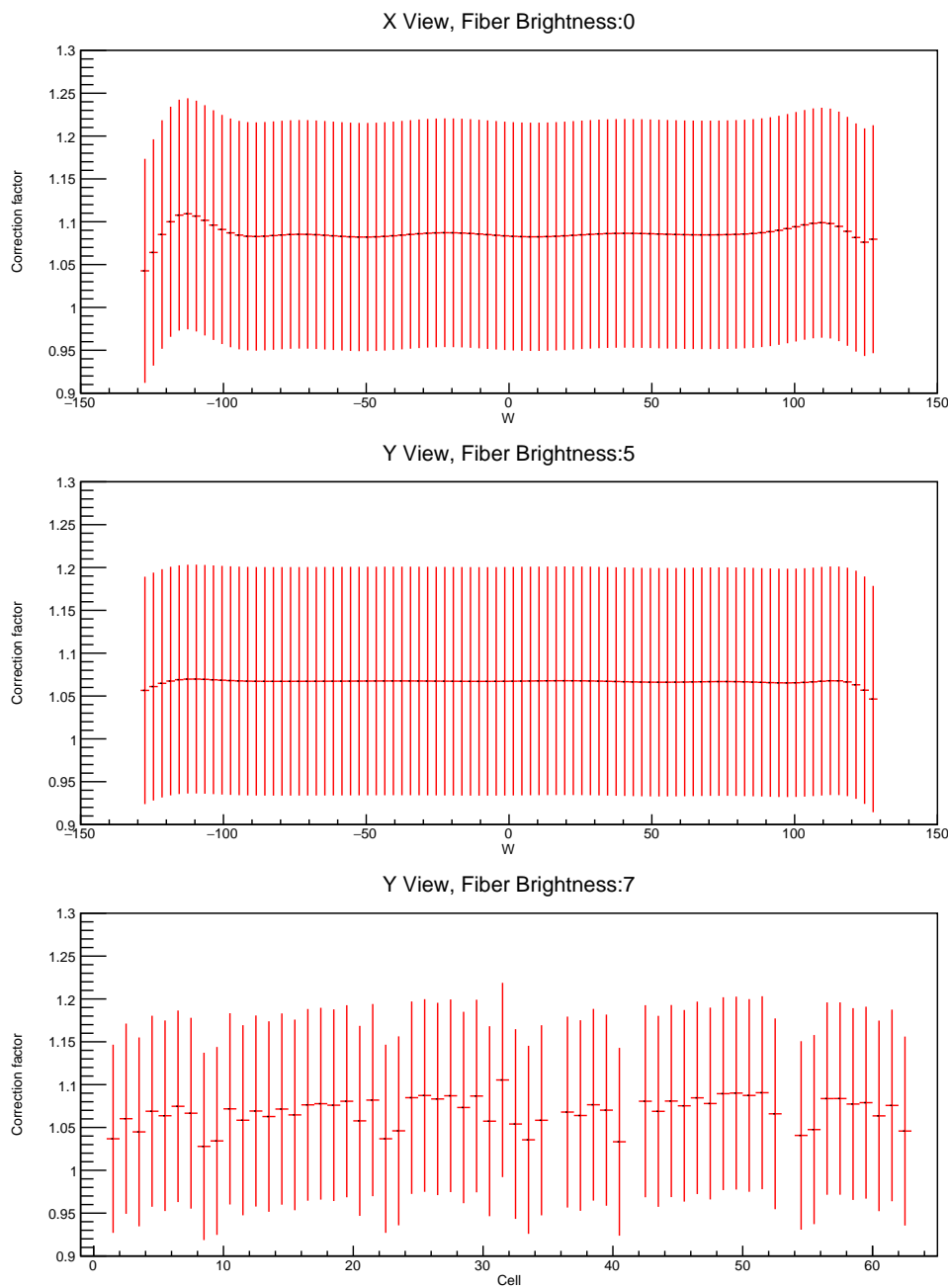


Figure 11: Examples of threshold and shielding corrections for the Test Beam detector

## 326 4.5 Period 2

327 The underfilled cells issue described in section 2 was present throughout period 2 data taking.  
 328 This can be clearly seen on figure 12, represented by the empty cells 31 and 63 in the horizontal  
 329 planes, which were marked as bad channels and therefore ignored during processing. This also  
 330 affects the neighbouring cells to the underfilled cells, which have fewer events due to the tricell  
 331 condition.

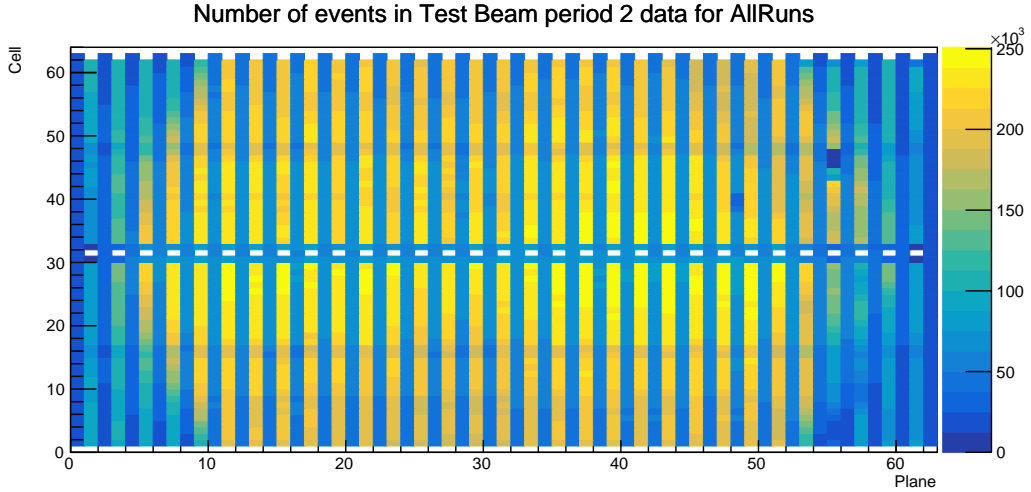


Figure 12: Distribution of events in the period 2 Test Beam data calibration sample.

332 There was also an issue of switched cables from the readout in plane 55 between cells 3  
 333 and 46 [28], which can also be seen on figure 12. This is manifested as fewer total number of  
 334 events in those cells and in their neighbours, again due to the tricell condition.

335 Officially, period 2 is divided into 6 epochs 2a - 2f, compared on figures 13, 14 and 15. The  
 336 epochs mostly differ in the use of various FEB firmwares, with epoch 2c being a trigger study  
 337 with paddles. As can be seen on the plots, the individual epochs vary only slightly, only in a  
 338 small normalization. We decided to use the entire period 2 without splitting it into any smaller  
 339 samples for calibration.

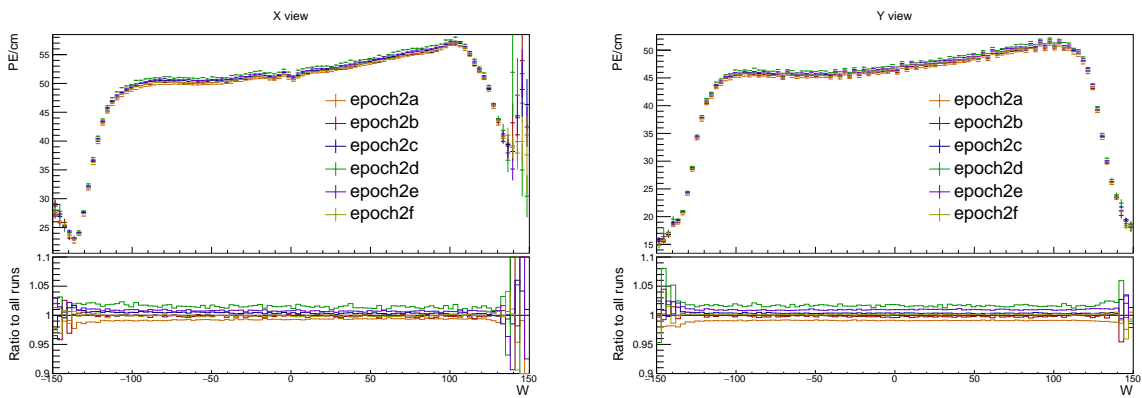


Figure 13: Uncorrected average energy response as a function of the position within a cell ( $w$ ) for epochs in period 2. It is clear that there is no significant difference between the various epochs.

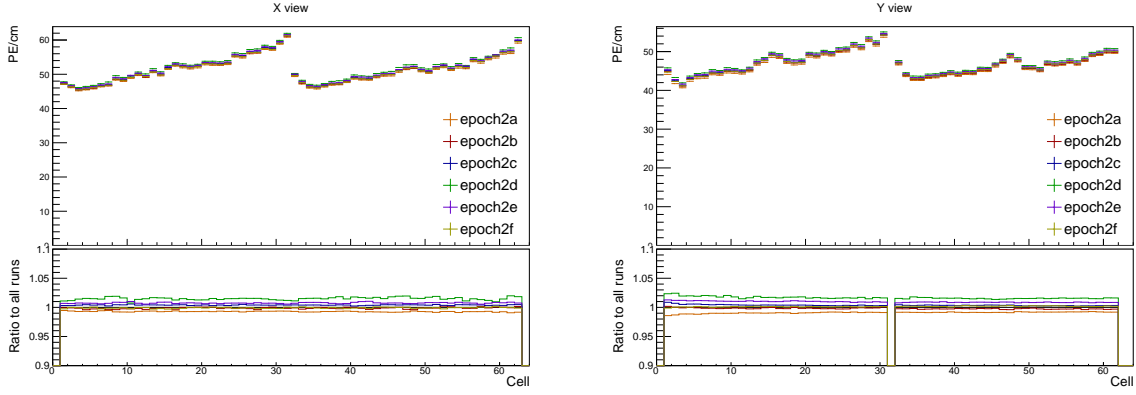


Figure 14: Uncorrected average energy response as a function of cells for epochs in period 2.

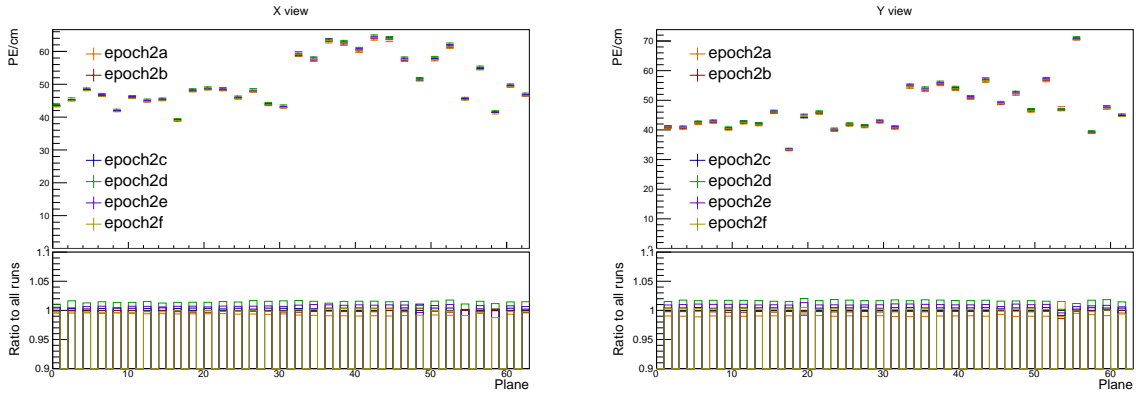


Figure 15: Uncorrected average energy response as a function of planes for epochs in period 2.

## 340 Period 2 relative calibration results

341 The results of the attenuation fit for period 2 are summarised on figure 16 showing the fitted  
342 response at the centre of each cell, or blank cell if the cell failed calibration.

343 Most of the cells have the expected response, as shown on the left plot of figure 17. Here  
344 the mean response in PE/cm slowly and approximately constantly rises towards the readout  
345 (right side of the plot) and drops down on the cell edges, marked with dashed lines.

346 Some cells have a non-flat response across the cell, with one or more regions with lower en-  
347 ergy response, as shown on the right plot of figure 17. These low regions are (almost certainly)  
348 a real physical effect caused by zipped, or possibly even twisted fibres [29], present in all of  
349 NOvA's detectors. Relative calibration corrects for this effect in data, but zipped fibres are not  
350 included in simulation, for any of the detectors. This could potentially cause issues with the  
351 ADC threshold in simulation.

352 Since the underfilled cells were marked as bad channels we didn't even attempt to calibrate  
353 them. Their neighbours have fewer events due to the tricell condition but majority of them  
354 pass the calibration condition, as shown on figure 18. The neighbouring cells in plane 1 don't  
355 pass the calibration due to low statistics and therefore large fluctuations, as shown on figure 19.  
356 This is likely due to a combination of the tricell condition and plane 1 being on the edge of the  
357 detector, which typically has fewer (accepted) hits than the center as shown on figure 12.

358 The left half of plane 55 has  $> 3 \times$  larger response than it's surrounding planes, as shown

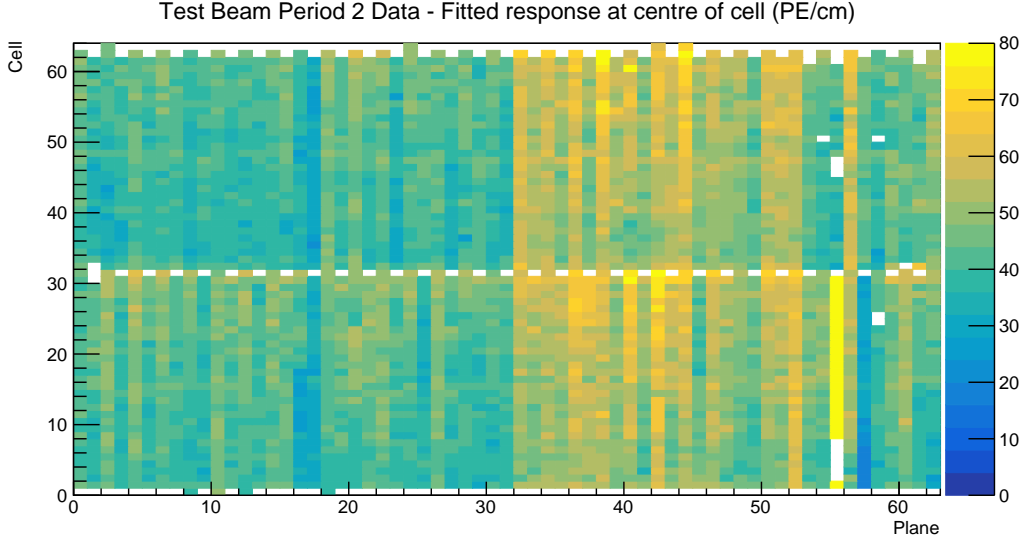


Figure 16: Overview of the relative calibration results for the Test Beam detector period 2 data. Each cell represents the result of the attenuation fit to the energy response in the centre of that cell. The blank cells are uncalibrated.

359 on the left plot of figure 20. Similarly, the left half of plane 57 has lightly lower response than  
 360 the surrounding planes, as shown on the right plot of figure 20. This is due to the corresponding  
 361 APDs/FEBs faultily recording different energy response than the real energy deposited in the  
 362 detector. Since this is present for all data, not only for the cosmic muons used for calibration,  
 363 it is important to correctly calibrate them. The issue can arise if these FEBs have been "faulty"  
 364 only for a limited time of the entire calibrated period. Since we are doing the attenuation fit on  
 365 the profile histograms, if an FEB records a standard response for half of the time and  $7\times$  larger  
 366 response for the seconds half, calibration is going to assume the response was  $4\times$  larger the  
 367 entire time, which is incorrect. Since both of these planes are in the back of the detector, we  
 368 decided to ignore this effect for period 2.

369 The swapped cables in plane 55 have almost no events, which affects both them and their  
 370 neighbours as shown of figure 21.

371 Several cells in the end of the Test Beam detector are uncalibrated due to bins on the edges  
 372 of the cell having an unusually high response, or no events at all, as shown on figure 22. It is  
 373 unknown if this is a real physical effect, possibly related to the fibres, or unfiltered noise hits,  
 374 or something else entirely. Since these cells are in the end of the detector, it is safe to ignore  
 375 them.

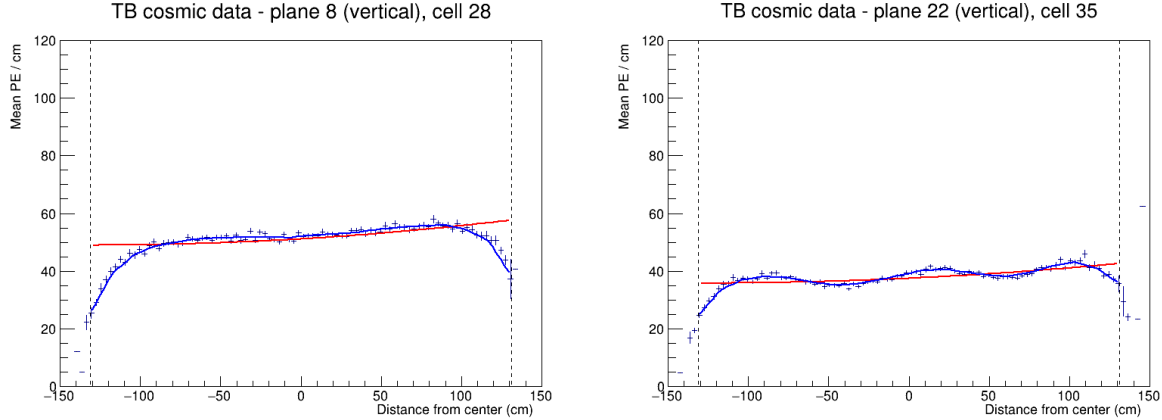


Figure 17: Attenuation fits for a selection of cells in period 2. Left plot shows an example of the standard energy deposition in the Test Beam. Right plot shows the effect of zipped fibres.

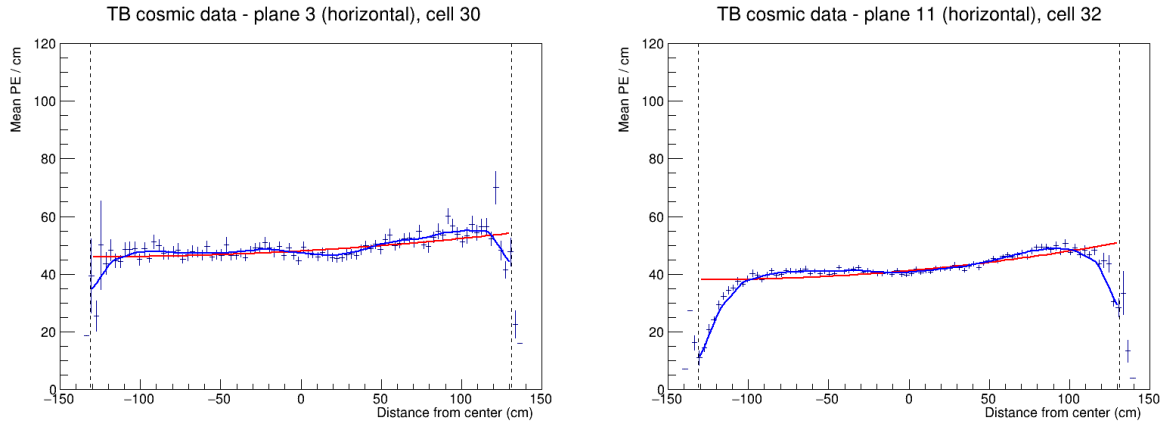


Figure 18: Fit to the energy response in period 2. The cells neighbouring the underfilled cells have fewer events and therefore larger fluctuations than the "usual" Test Beam cell.

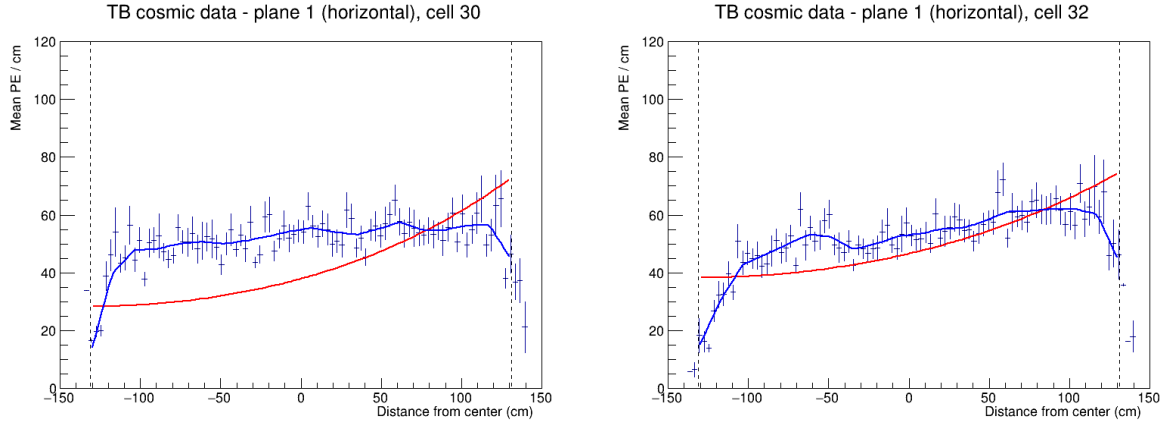


Figure 19: Fit to the energy response in period 2. The neighbouring cells to the underfilled cells in plane 1 are uncalibrated due to low statistics.

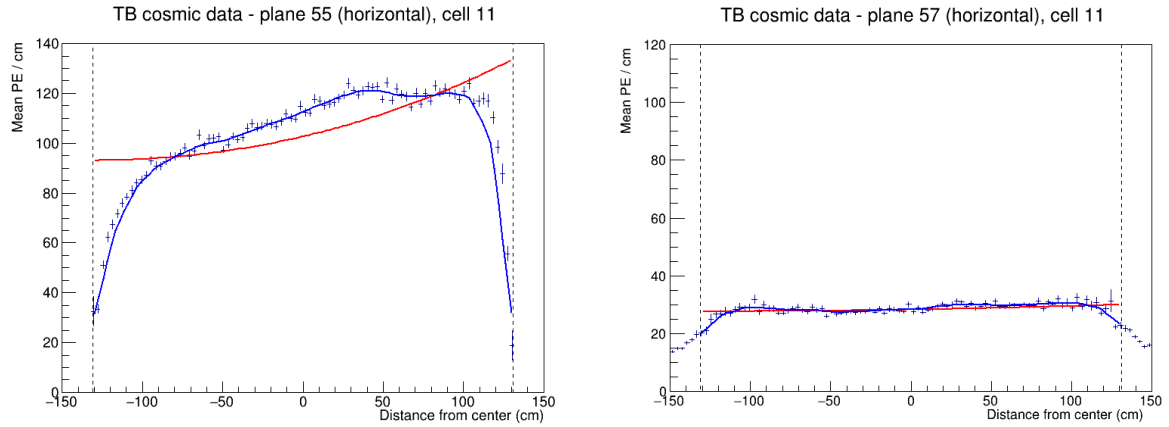


Figure 20: Fit to the energy response in period 2. Lower halves of planes 55 and 57 have a different scale of energy response than the surrounding planes.

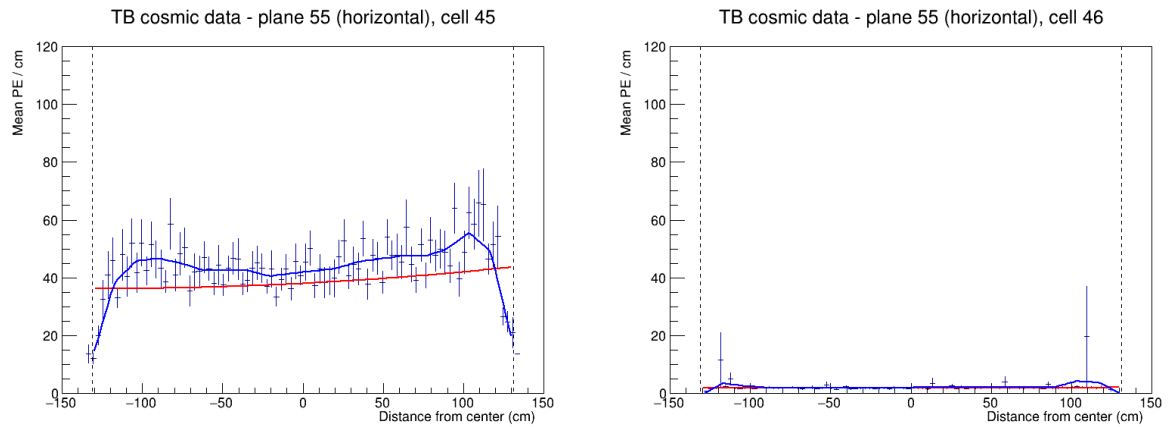


Figure 21: Fit to the energy response in period 2. Cells with swapped readout cables have almost no recorded events as shown on the right plot. This also affect their neighbouring cells due to the tricell condition as shown on the left plot.

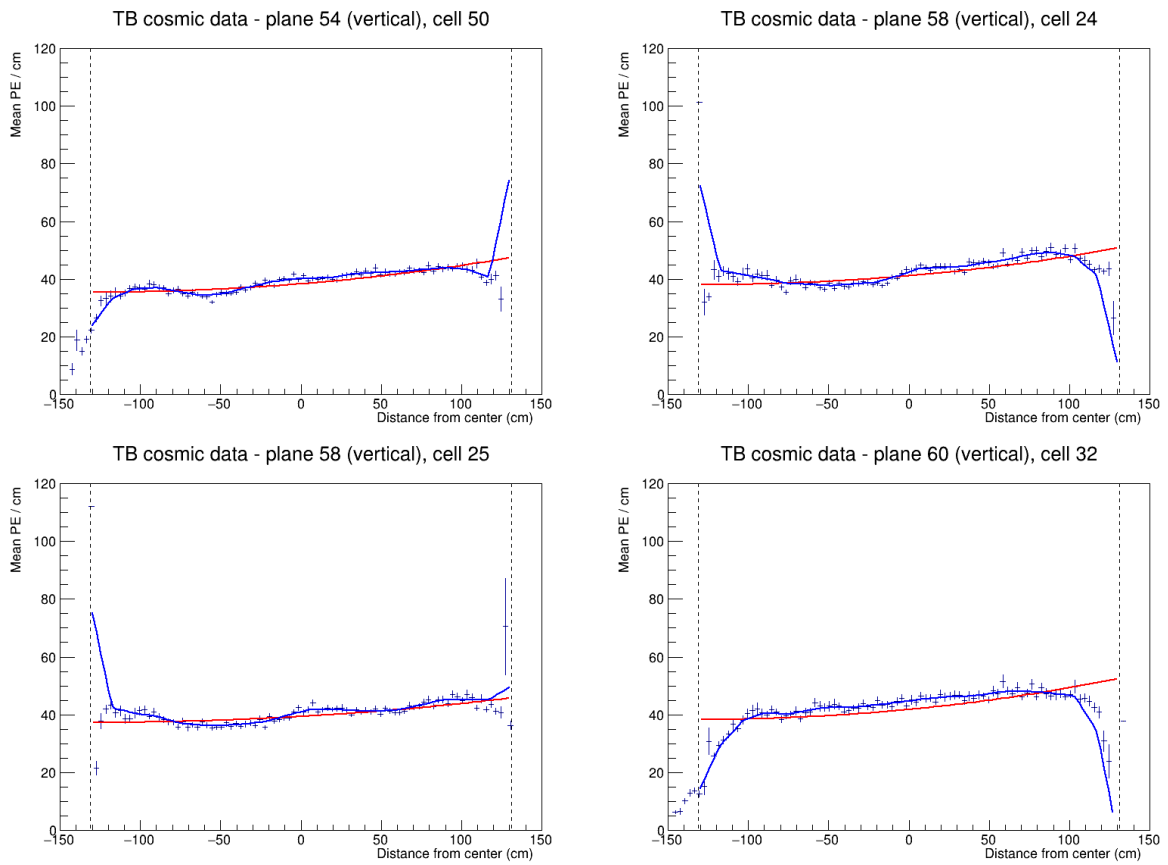


Figure 22: Fit to the energy response in period 2. Examples of cells that have an unusually high or low energy response at the edge of the cell. These cells are not calibrated.

<sup>376</sup> **4.6 Period 3**

<sup>377</sup> The underfilled cells were refilled (or overfilled) during the period 3 data taking. This was the  
<sup>378</sup> main motivation for dividing period 3 into individual epochs as shown on table 4. One more  
<sup>379</sup> major event that could impact the Test Beam data is the replacement of several faulty FEBs,  
<sup>380</sup> which motivated the creation of epoch 3e.

|          |                               |  |
|----------|-------------------------------|--|
| Epoch 3a | January 12 <sup>th</sup> 2021 | Underfilled cells  |
| Epoch 3b | April 21 <sup>st</sup> 2021   | Overfilling the back 9 horizontal planes and the 7th horizontal plane from the front                                 |
| Epoch 3c | April 27 <sup>th</sup> 2021   | Overfilling of the 15 front horizontal planes (except the 7th, which was already done) and the 14th horizontal plane |
| Epoch 3d | April 30 <sup>th</sup> 2021   | Overfilling of the remaining 8 horizontal planes   |
| Epoch 3e | May 12 <sup>th</sup> 2021     | FEB swaps  |

Table 4: Test Beam period 3 epochs, their start dates and the reason for their separation.

<sup>381</sup> The refilling of the underfilled cells can be clearly seen on the cell hits distribution on figure  
<sup>382</sup> 23 and on the distribution of energy deposition across horizontal cells (Y view) on figure 25.

<sup>383</sup> From the cell hits distributions we can also see there are a few channels (cells) that were  
<sup>384</sup> likely dead for a certain time and weren't recording the same number of events as the surround-  
<sup>385</sup> ing cells. This is specifically plane 48, cell 39 in all of period 3 and plane 18, cell 31 in epochs  
<sup>386</sup> 3d and 3e.

<sup>387</sup> The energy distributions across vertical cells and planes (X view) on figures 25 and 26  
<sup>388</sup> shows, that the top half of plane 58 has a very distinctly different energy deposition compared  
<sup>389</sup> to the rest of the cells, while having the same number of events, as can be seen on figure 23.  
<sup>390</sup> This is the most impactful of the faulty FEBs replaced for Epoch 3e.

<sup>391</sup> From these discussion, we have decided to calibrate epochs 3a, 3b and 3c together (all  
<sup>392</sup> epochs containing any underfilled cells) and separately calibrated epochs 3d and 3e. The faulty  
<sup>393</sup> FEB in plane 58 is far enough in the back of the detector that we didn't find it necessary to  
<sup>394</sup> calibrate epochs 3d and 3e separately. Also epochs 3b and 3c only contain a few days worth of  
<sup>395</sup> data, which wouldn't be enough for a successful attenuation fit.

<sup>396</sup> **Combined epochs 3a, 3b and 3c relative calibration results**

<sup>397</sup> The results of the attenuation fit are summarised on figure 27 showing cell × plane distribution  
<sup>398</sup> of the fitted response at the centre of each cell.

<sup>399</sup> We can see that some of the underfilled cells that have been refilled for epochs 3b or 3c are  
<sup>400</sup> now calibrated thanks to including them into the same attenuation fit. An example of energy  
<sup>401</sup> deposition in such a cell is on the left plot of figure 28.

<sup>402</sup> Same as in period 2 most of the neighbouring cells to the underfilled cells are calibrated,  
<sup>403</sup> except for cell 32 in plane 1, shown on the right of figure 28, which is also affected by the low  
<sup>404</sup> statistics at the edges of the detector.

<sup>405</sup> There is a couple of notably faulty FEBs with a different energy response than their neigh-  
<sup>406</sup> bours. Besides the expected top half of plane 58, which has about 5× larger response than the

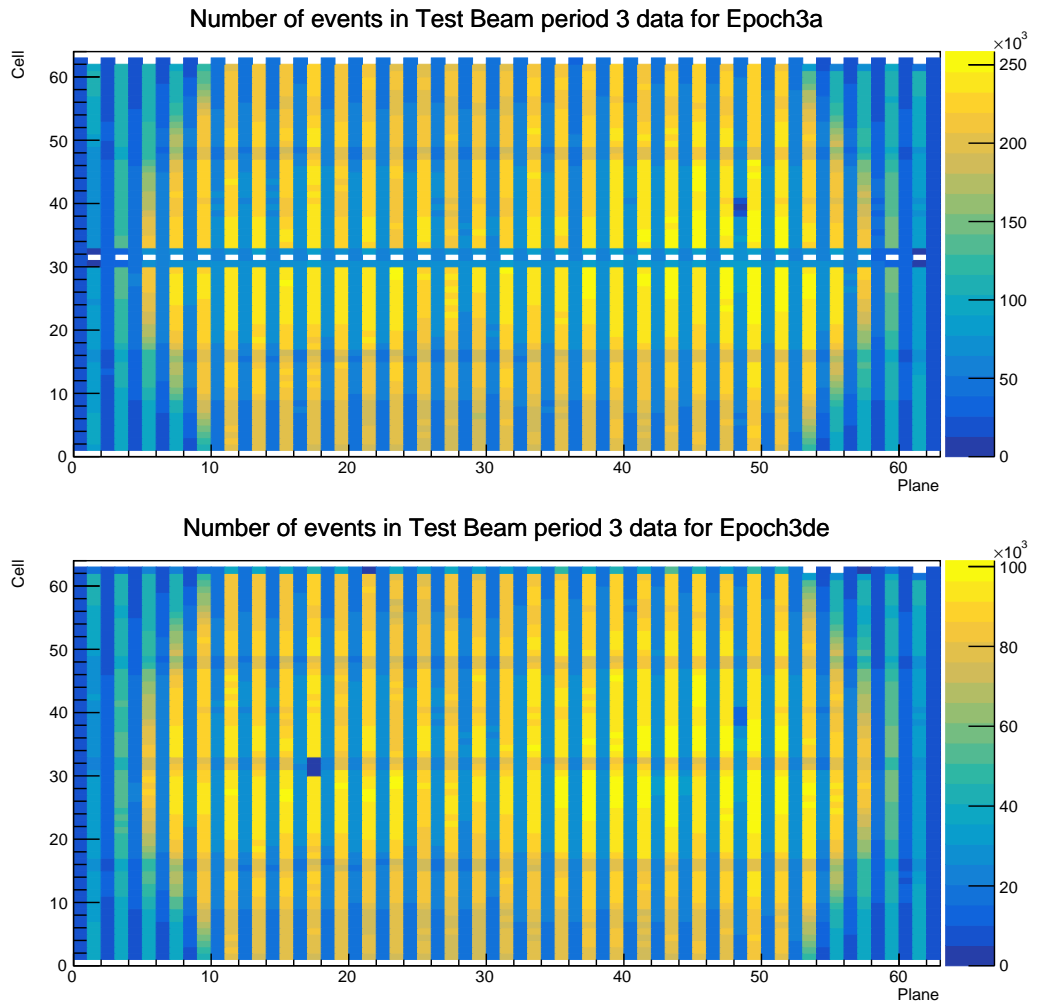


Figure 23: Distribution of events in the period 3 Test Beam data calibration sample. Comparison of Epoch 3a data before the refilling of the underfilled cells and Epoch 3de (combination of Epochs 3d and 3e) after the full refilling.

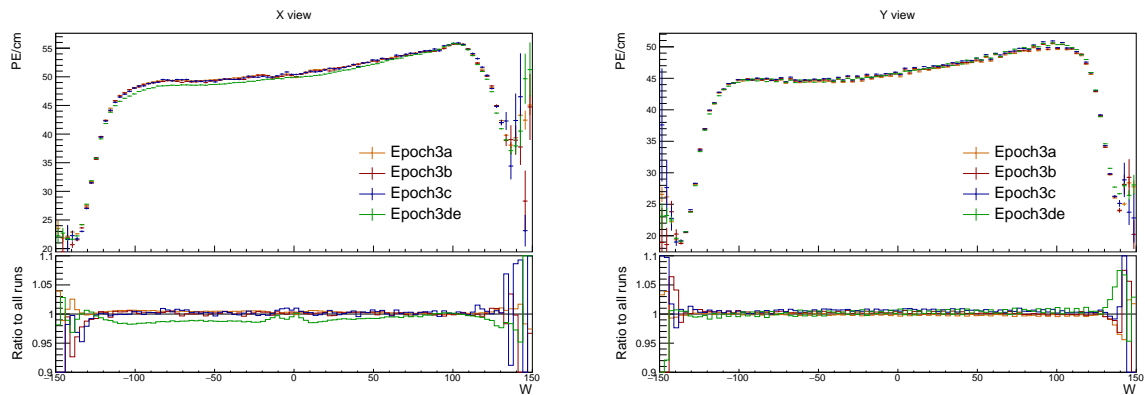


Figure 24: Uncorrected average energy response as a function of the position within a cell ( $w$ ) for epochs in period 3.

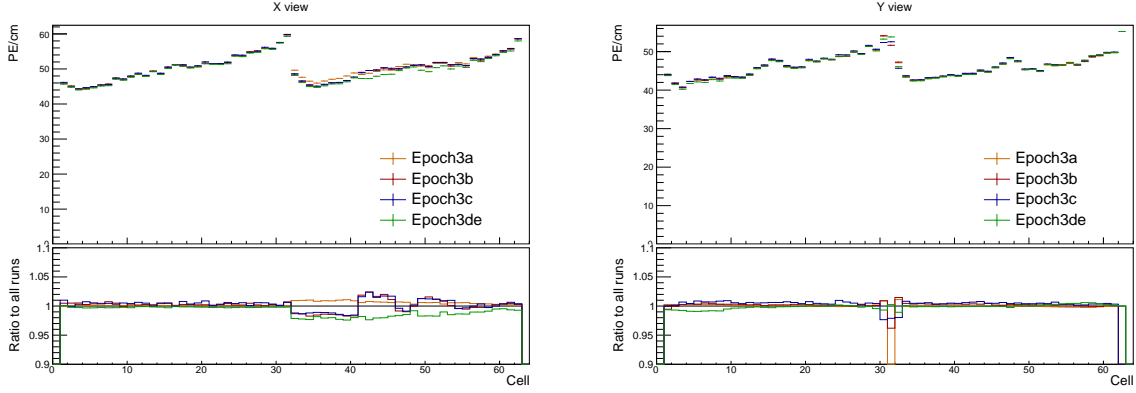


Figure 25: Uncorrected average energy response as a function of cells for epochs in period 3.

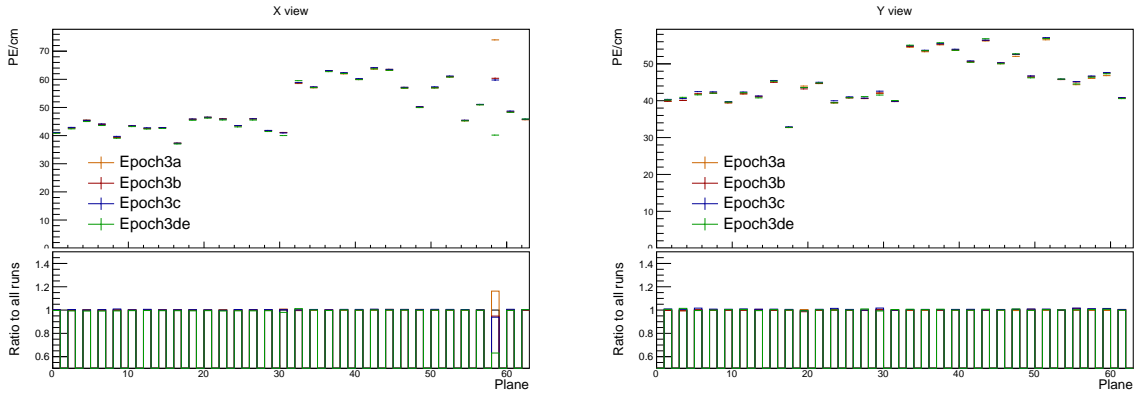


Figure 26: Uncorrected average energy response as a function of planes for epochs in period 3.

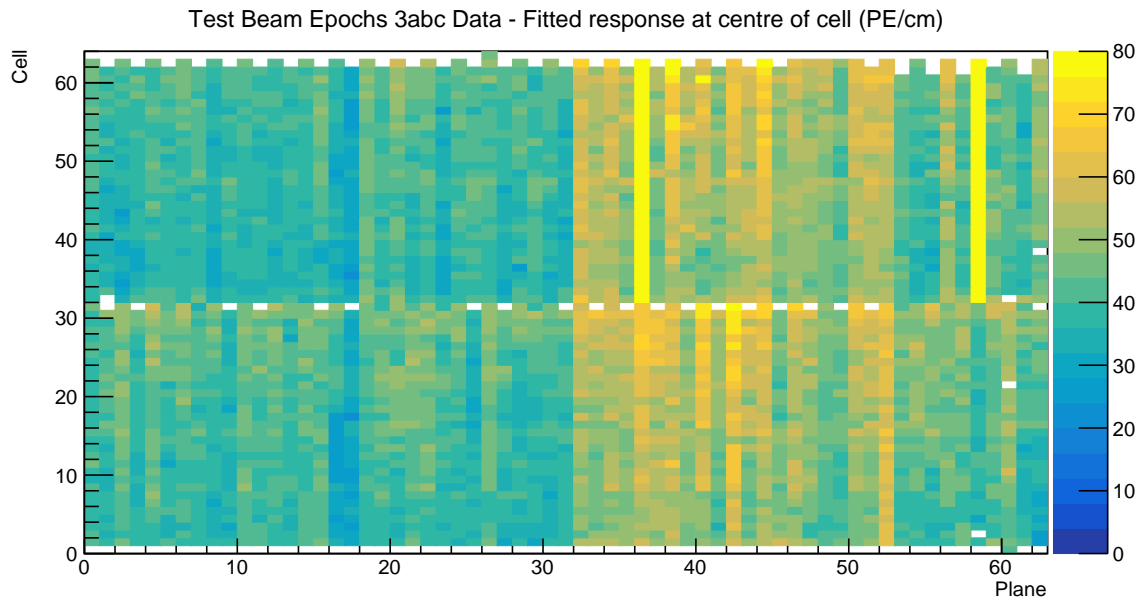


Figure 27: Overview of the relative calibration results for the Test Beam detector period 3, combined epochs 3a, 3b and 3c data. Each cell represents the result of the attenuation fit to the energy response in the centre of that cell. The blank cells are uncalibrated.

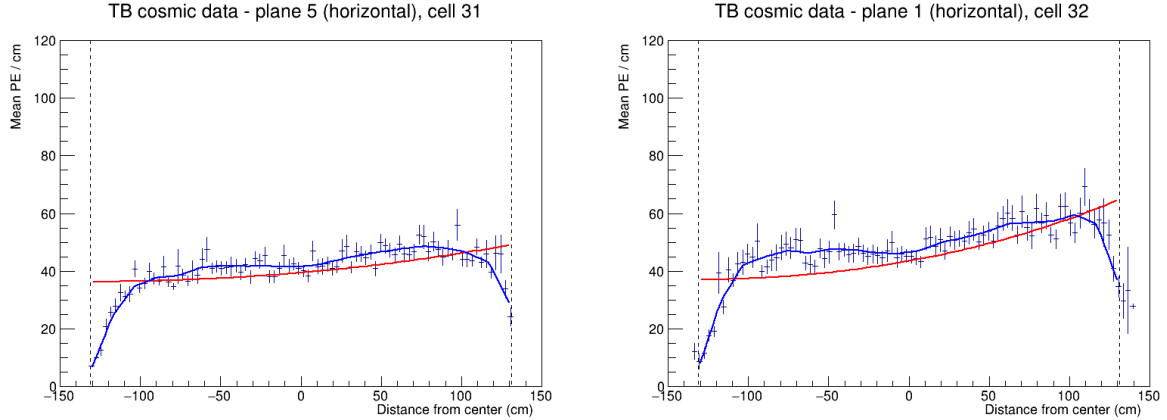


Figure 28: Fit to the energy response in epochs 3 a, b and c. Some underfilled cells that have been refilled in epochs 3b and 3c are now calibrated as shown on the left plot. Cell 32 in plane 1 is the only neighbouring cell to the underfilled cell that didn't manage to get calibrated due to low number of events.

407 usual, it's also the top half of plane 36, which has about  $2.5 \times$  larger response as its neighbours.  
 408 This could mean that the FEB in plane 36 was faulty only for a limited time compared to the  
 409 FEB in plane 58. The energy deposition for these cells is shown on figure 29.

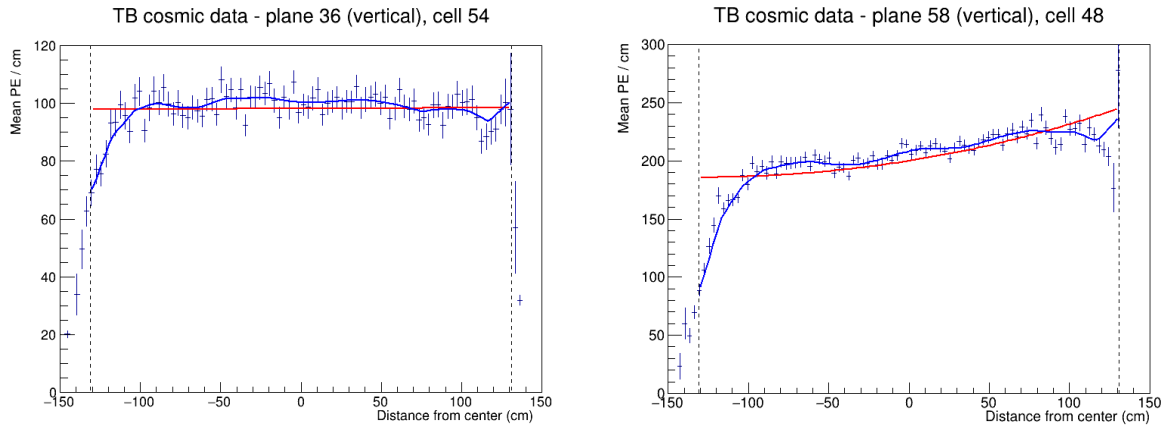


Figure 29: Fit to the energy response in epochs 3 a, b and c. The most obvious faulty FEBs that have a significantly larger energy response than their neighbours.

410 Similarly as in period 2, there are a few cell in the back of the detector that have a sharp  
 411 rise in the energy response at the edge of the cell, which causes them to be uncalibrated. This  
 412 can be seen on figure 30.

#### 413 **Combined epochs 3d and 3e relative calibration results**

414 The results of the attenuation fits for epochs 3 d and e are shown on figure 31. There we can  
 415 see the expected uncalibrated cells in plane 17 related to the dead channel (or possibly still  
 416 underfilled cell). The energy deposition for this cell and one of its neighbours is shown on  
 417 figure 32.

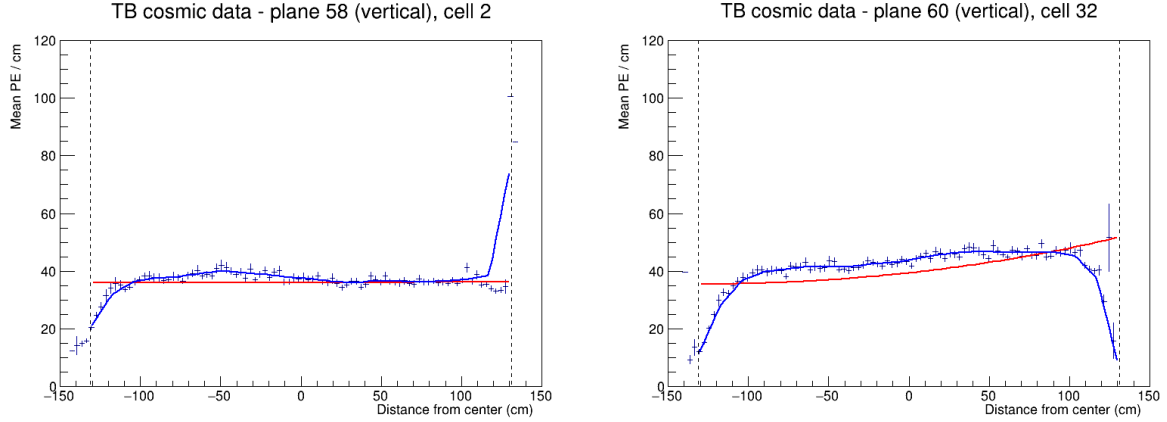


Figure 30: Fit to the energy response in epochs 3 a, b and c. Some cells are not calibrated due to large fluctuations at one edge of the cells.

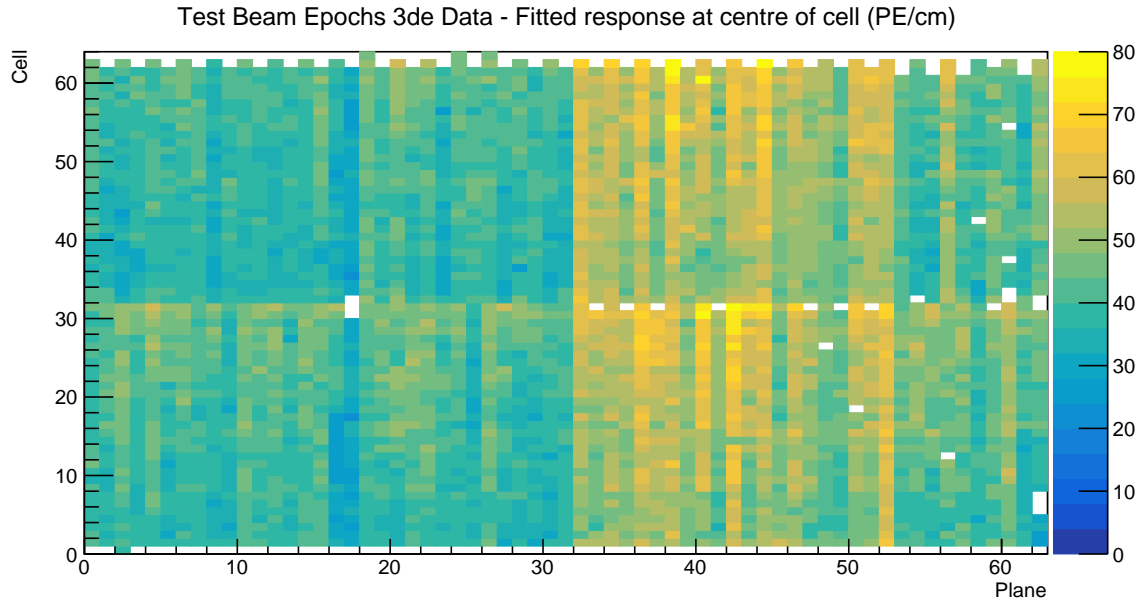


Figure 31: Overview of the relative calibration results for the Test Beam detector period 3, combined epochs 3d and 3e data. Each cell represents the result of the attenuation fit to the energy response in the centre of that cell. The blank cells are uncalibrated.

418      Epochs 3 d and e should have all the previously underfilled cells now refilled, but as can be  
 419      seen on figure 31, there's several of these cells that are still uncalibrated. The energy deposition  
 420      in these cells is shown on figure 33. We can see that these cells have a fairly large discrepancy  
 421      between the left and right side of the cells. This is caused by using different scintillator oils for  
 422      the initial filling of the cells and for the refilling. Specifically, these cells have been initially  
 423      filled with the Ash River and the Texas oils, which have higher energy depositions compared  
 424      to the NDOS oil that was used for the refilling. These oils clearly didn't mix properly which  
 425      causes a different energy deposition in different parts of the cells. Since this is a physical effect  
 426      that should be accounted for in the calibration and as we can see the fits are actually performing  
 427      pretty well and are just confused by the unusual shape. We have therefore decided to manually

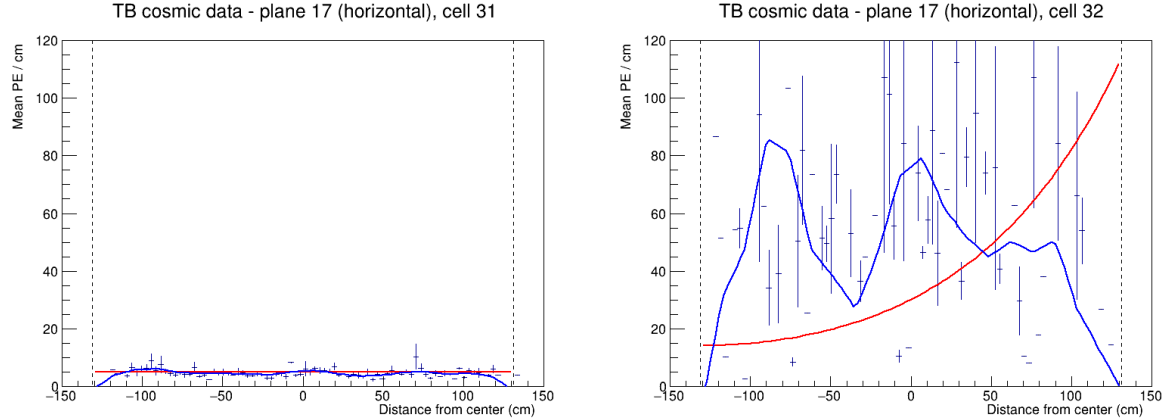


Figure 32: Fit to the energy response in epochs 3 d and e. Possibly dead channel or still underfilled cell.

428 change the  $\chi^2$  inside the cvs tables (results of the attenuation fits), so that the  $\chi^2 < 0.2$  and  
429 these cells are considered calibrated.

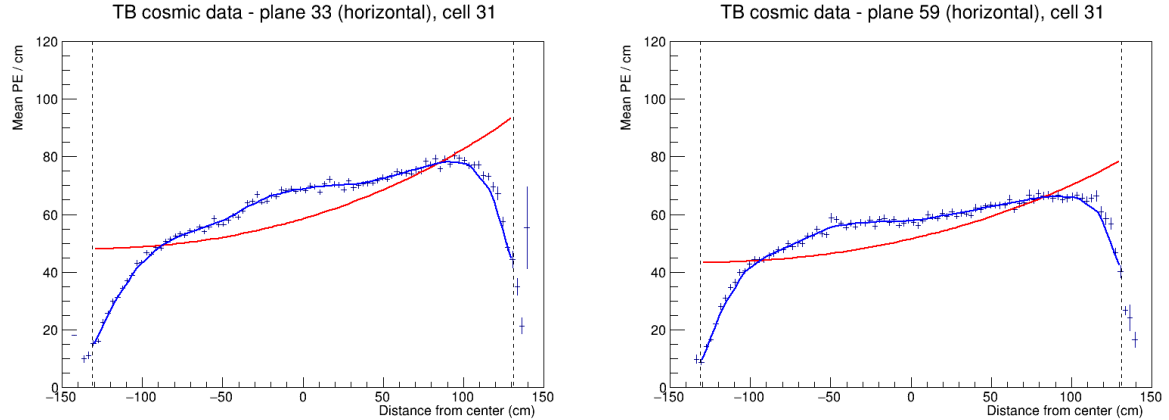


Figure 33: Fit to the energy response in epochs 3 d and e. The scintillator oil used for refilling of the underfilled cells has lower energy response than the oil used for the initial filling. These oils didn't mix properly causing a different energy response in the left and right side of the cell.

430 Some of the cells in the back of the detector have a rise, or drop in energy deposition at the  
431 edge of the cell, as can be seen on figure 34. This is similar to the effect seen in period 2 and  
432 epochs 3abc and since it's again concentrated in the end of the detector we ignored these cells  
433 and left them uncalibrated.

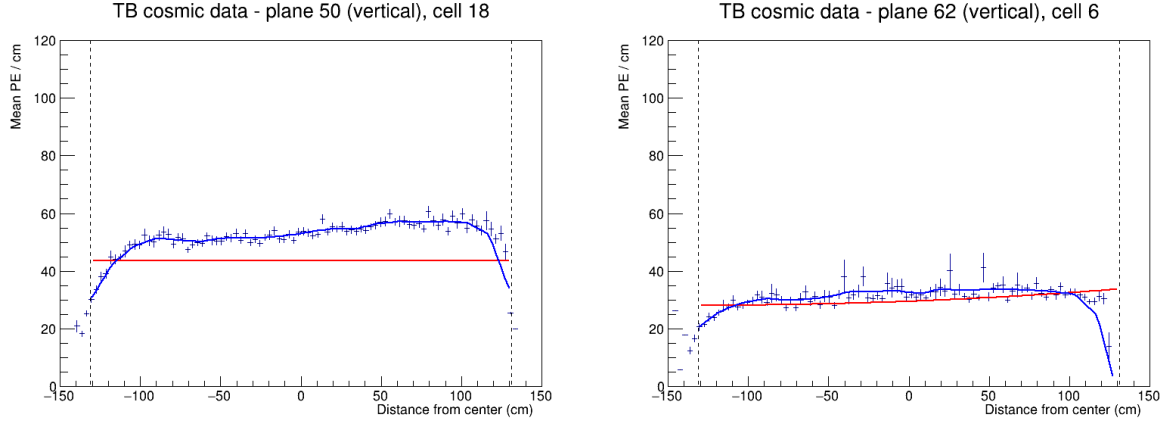


Figure 34: Fit to the energy response in epochs 3 d and e. Some cells have a drop, or a rise of energy response at the edge of the cell. This can be cause by low statistics.

## 4.7 Period 4

The period 4 Test Beam data taking period is the best data we managed to collect with almost an ideal condition of the detector. There's only a few commissioning runs in the very beginning, which uncovered some dead channels or faulty FEBs that have been fixed. These runs make epoch 4a shown on the top plot of figure 35.

There has also been a cell masking study [reference], during which we masked parts of the front of the detector to help with FEB saturation. We can clearly see this on the middle plot of figure 35.

Figures 36, 37 and 38 show that the epoch 4a and the cell masking study did have a noticeable impact on the energy deposition across the detector. We have therefore decided to ignore these runs and only use the rest of the period 4 data for the calibration.

### Period 4 relative calibration results

Results of the attenuation fits for period 4 are summarised on figure 39.

We can see that majority of the detector is calibrated, besides some cells on the edge of the detector, a few formerly underfilled cells (left plot on figure 40) and one cell with an unusually high response at the edge of the cell (right plot on figure 40). We treated the formerly underfilled cells the same way as in epochs 3 d and e, by manually changing their  $\chi^2$  to be  $< 0.2$  and therefore making them calibrated.

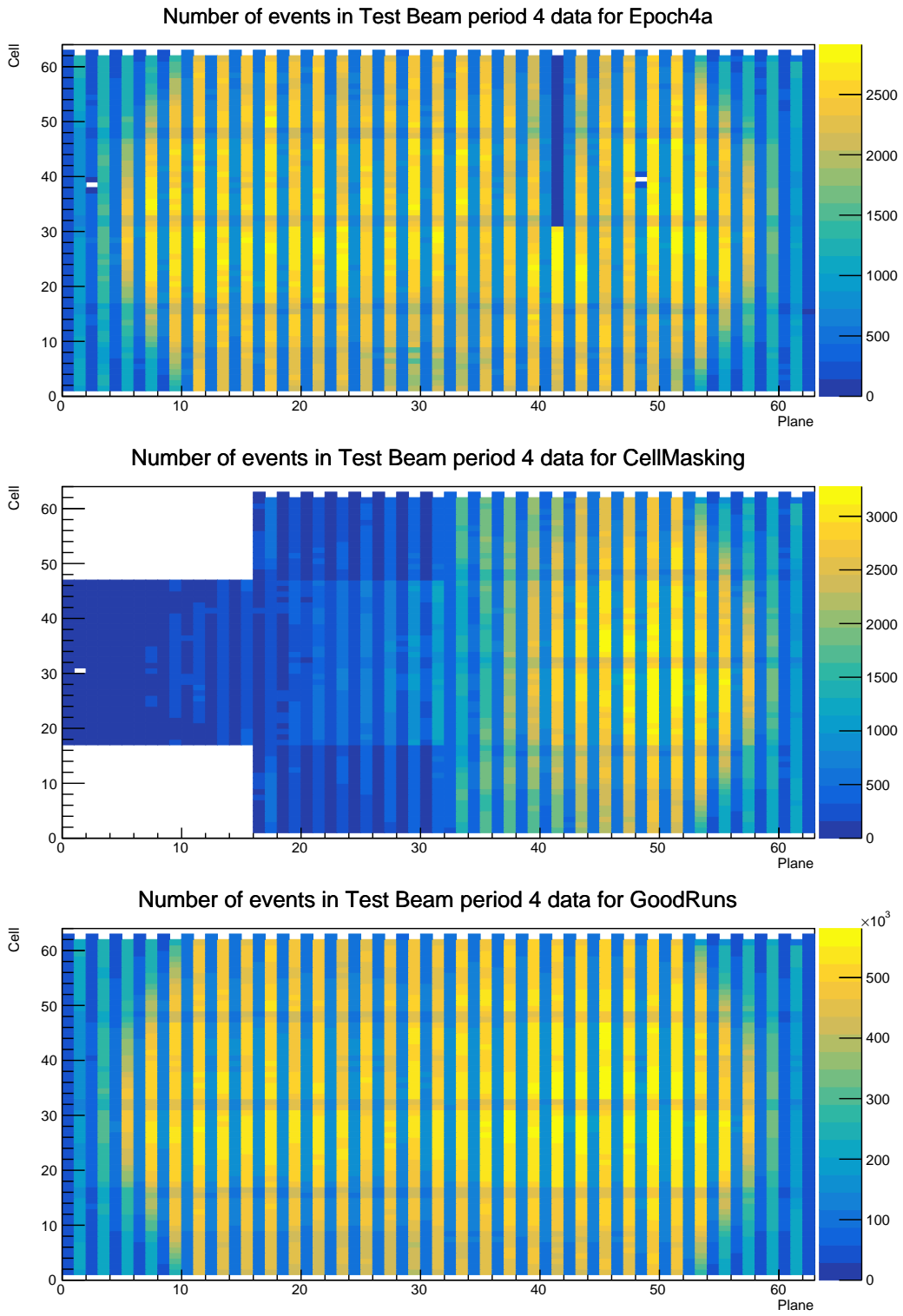


Figure 35: Distribution of events in the Test Beam period 4 data calibration sample. The top plot shows the first three commissioning runs, the middle plot the status of the detector during the Cell Masking studies and the bottom plot shows the rest.

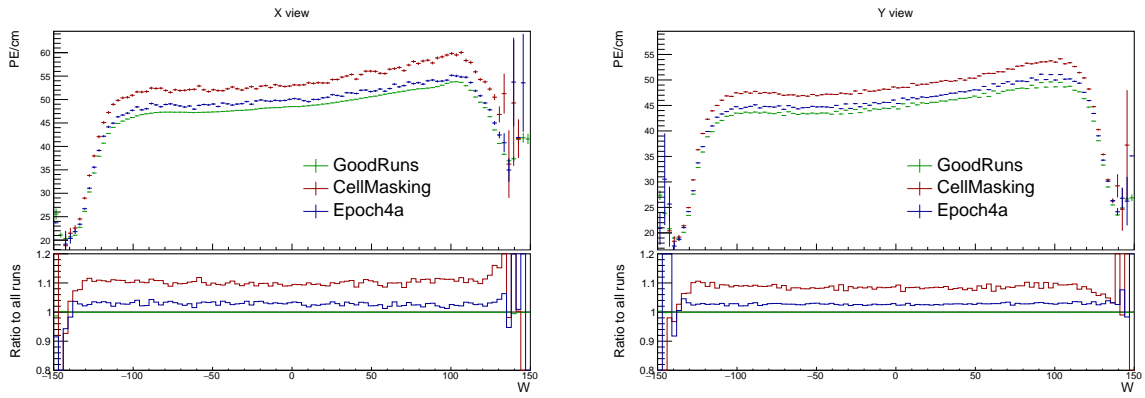


Figure 36: Uncorrected average energy response as a function of the position within a cell ( $w$ ) for epochs in period 4.

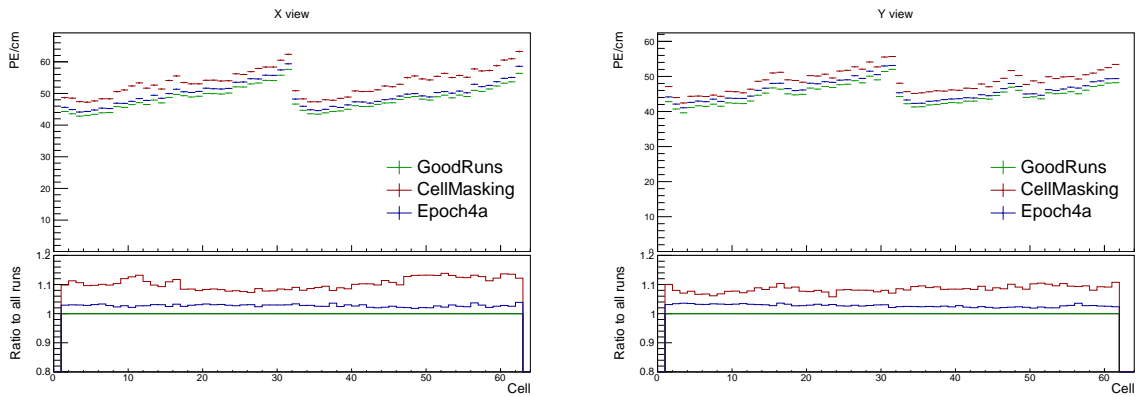


Figure 37: Uncorrected average energy response as a function of cells for epochs in period 4.

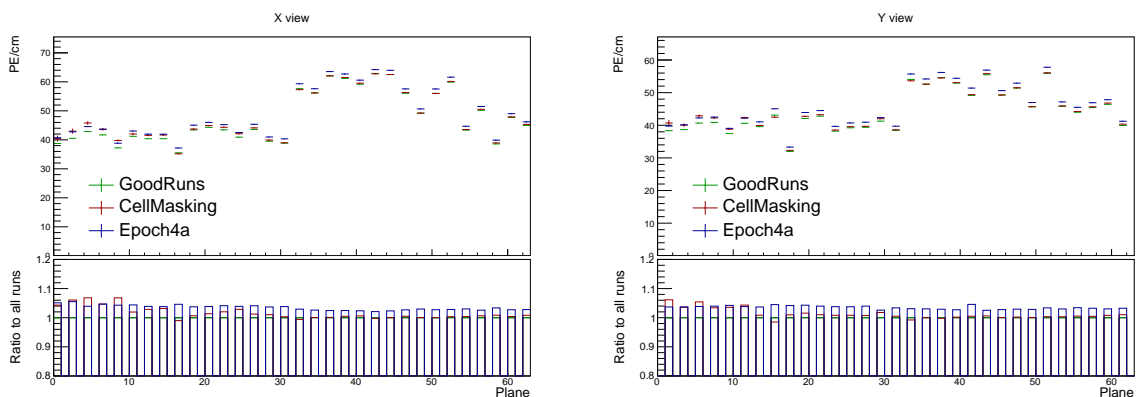


Figure 38: Uncorrected average energy response as a function of planes for epochs in period 4.

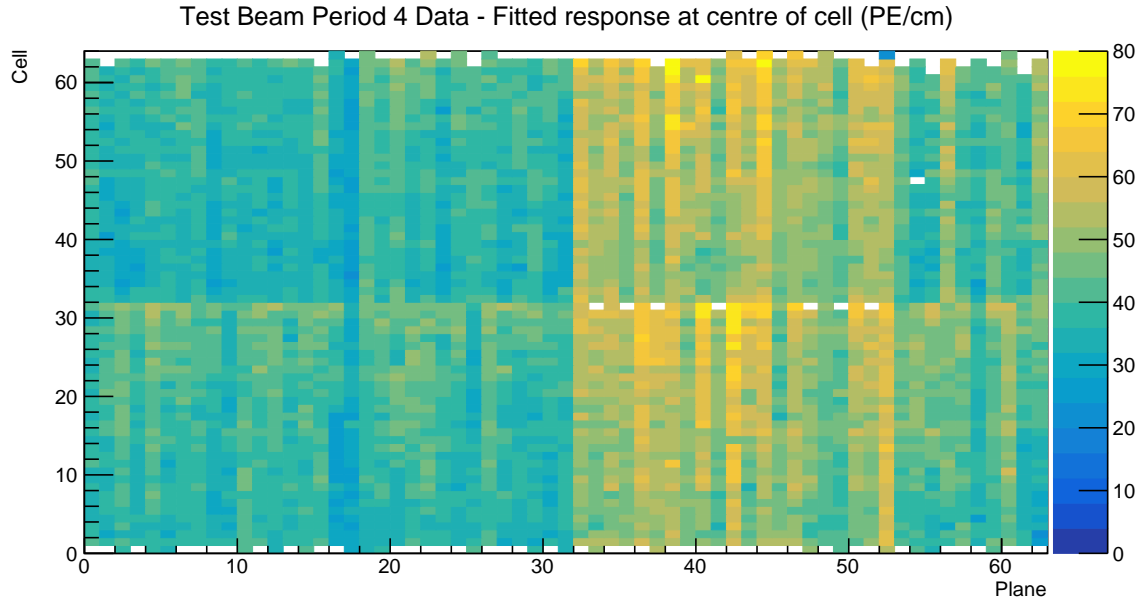


Figure 39: Overview of the relative calibration results for the Test Beam detector period 4 data. Each cell represents the result of the attenuation fit to the energy response in the centre of that cell. The blank cells are uncalibrated.

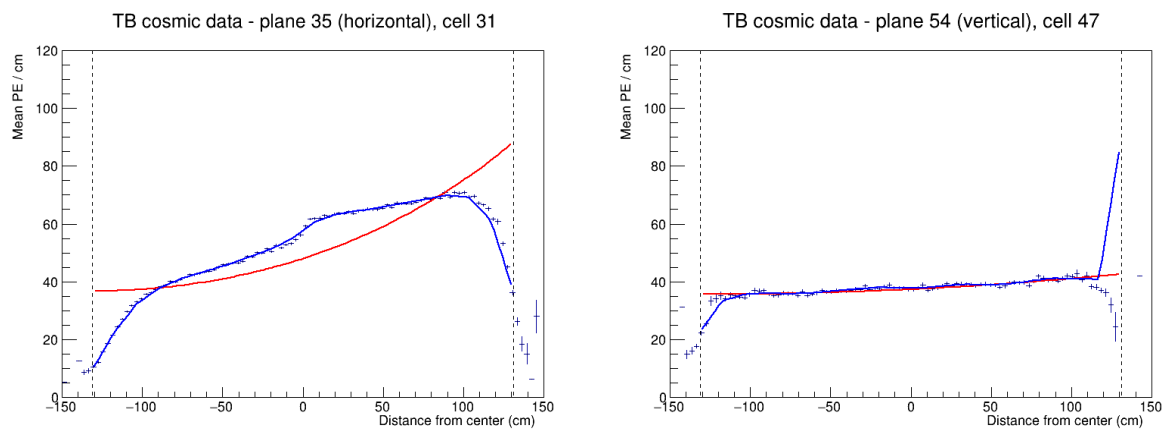


Figure 40: Fit to the energy response in period 4. Previously underfilled cells refilled with a scintillator of a different quality causing an unusual distribution of energy deposition (left). Unusually high energy response at the edge of the cell 47 (right).

<sup>452</sup> **4.8 Absolute calibration results**

<sup>453</sup> TO DO: add description of the absolute calibration results, correct the table to fit the page

| Sample          | NHitsx    | MEUx  | NHitsy    | MEUy  | MEU   | MEU Err  | TrueE/dx | tE/dx Err |
|-----------------|-----------|-------|-----------|-------|-------|----------|----------|-----------|
| epoch 3abc data | 2.638e+05 | 38.49 | 1.621e+06 | 39.4  | 38.94 | 0.006758 | 1.772    | 0.000238  |
| epoch 3de data  | 1.049e+05 | 38.63 | 6.725e+05 | 39.42 | 39.02 | 0.01048  | 1.772    | 0.000238  |
| period 2 data   | 2.322e+05 | 38.7  | 1.413e+06 | 39.4  | 39.05 | 0.007252 | 1.772    | 0.000238  |
| period 4 data   | 5.268e+05 | 38.63 | 3.316e+06 | 39.4  | 39.01 | 0.004703 | 1.772    | 0.000238  |
| simulation      | 2.829e+05 | 40.17 | 1.842e+06 | 39.93 | 40.05 | 0.006418 | 1.772    | 0.000238  |

<sup>454</sup>

<sup>455</sup> **4.9 Results**

<sup>456</sup> TO DO: talk about where are the results and what is the final calibration tag

<sup>457</sup> **4.10 Validation**

<sup>458</sup> TO DO: describe the validation plots and possibly add more plots

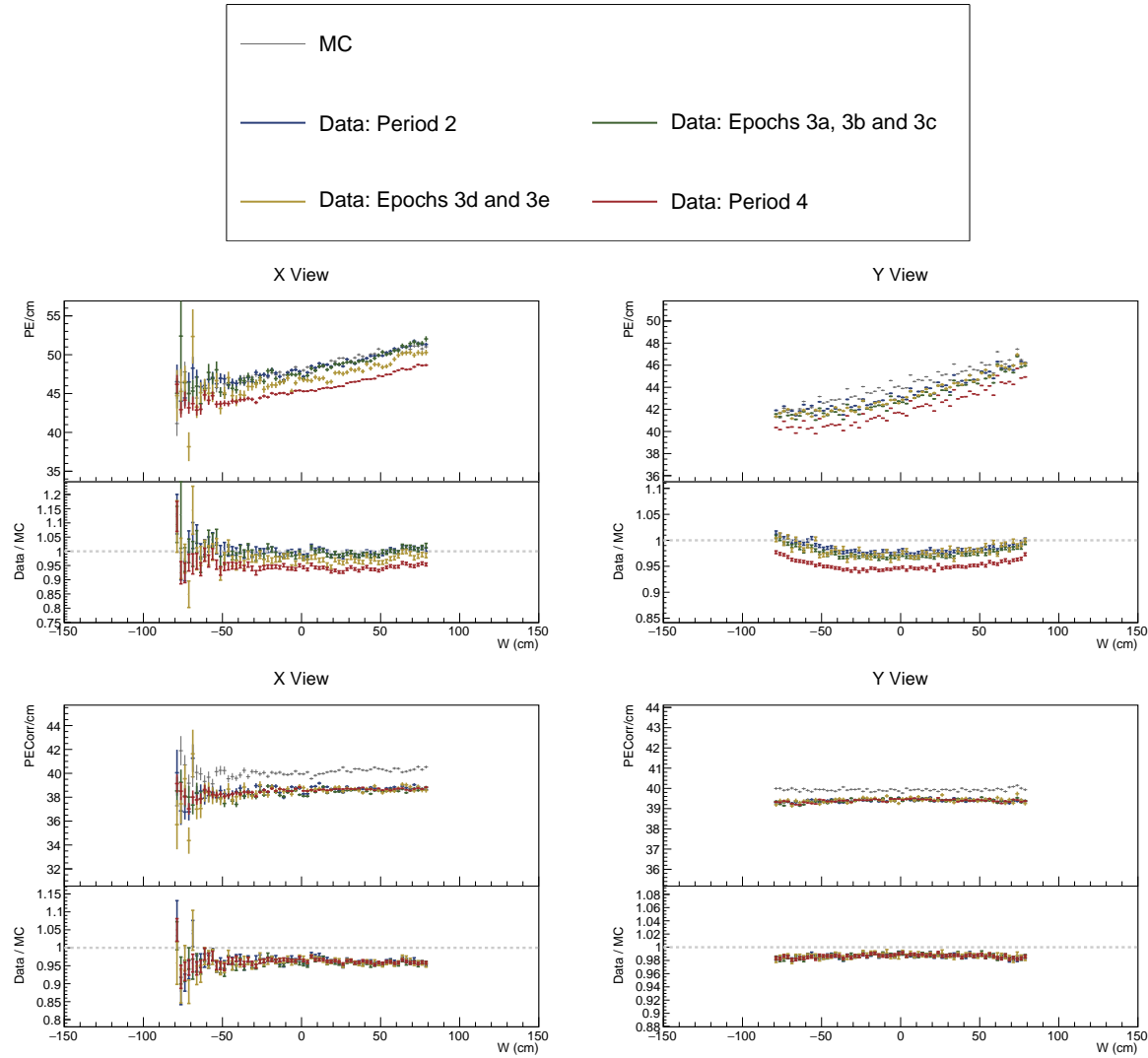


Figure 41: ...

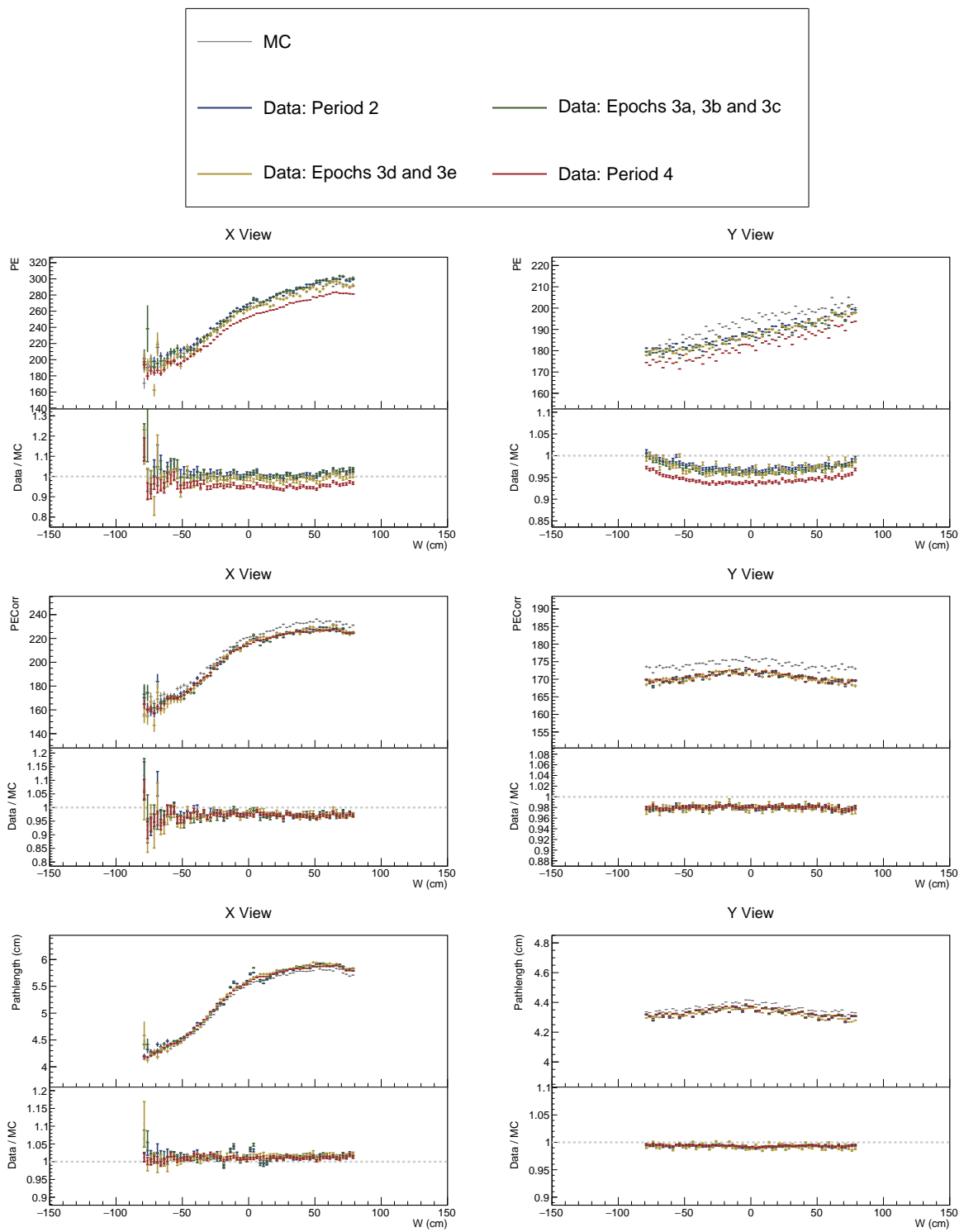


Figure 42: ...

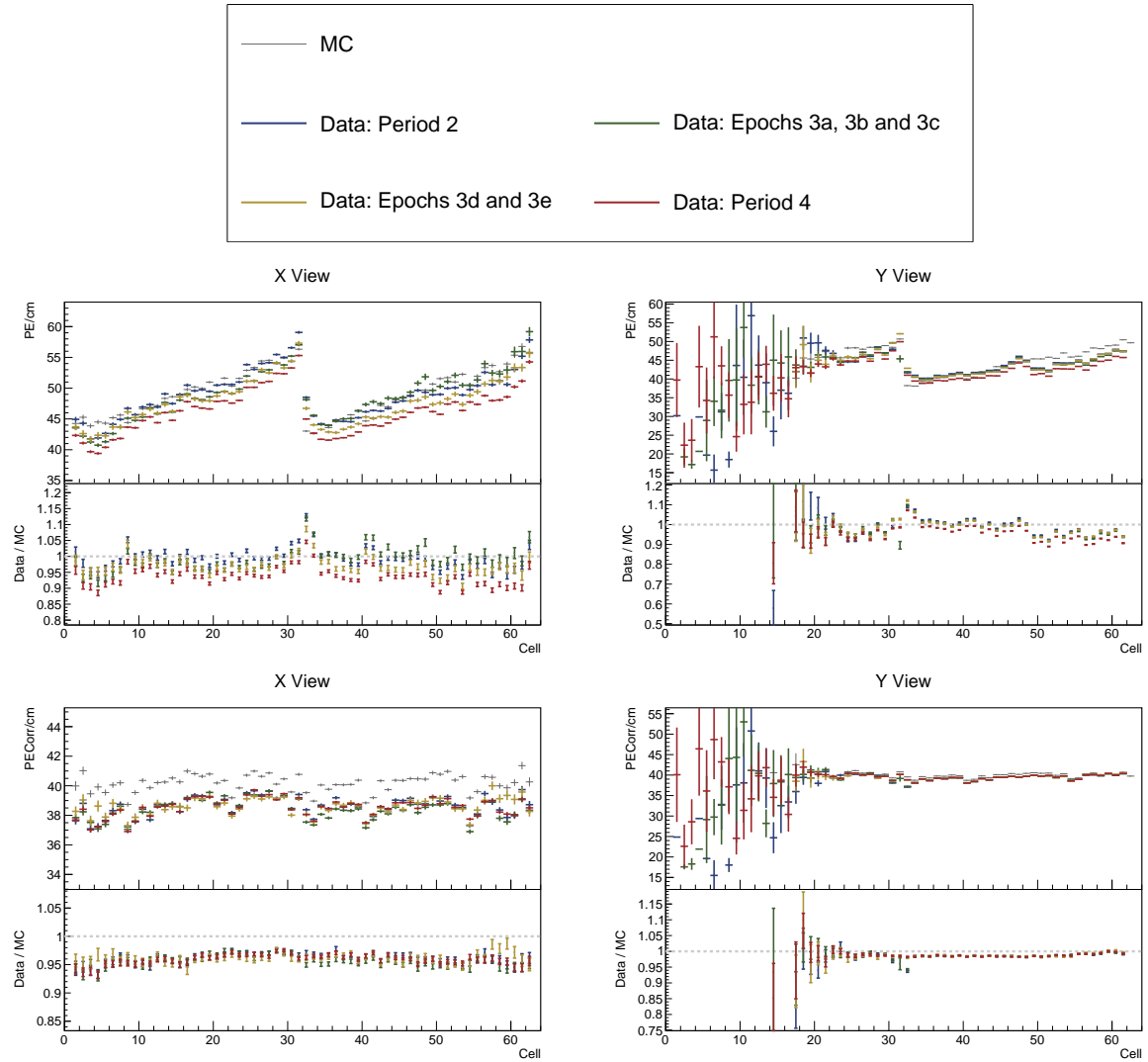


Figure 43: ...

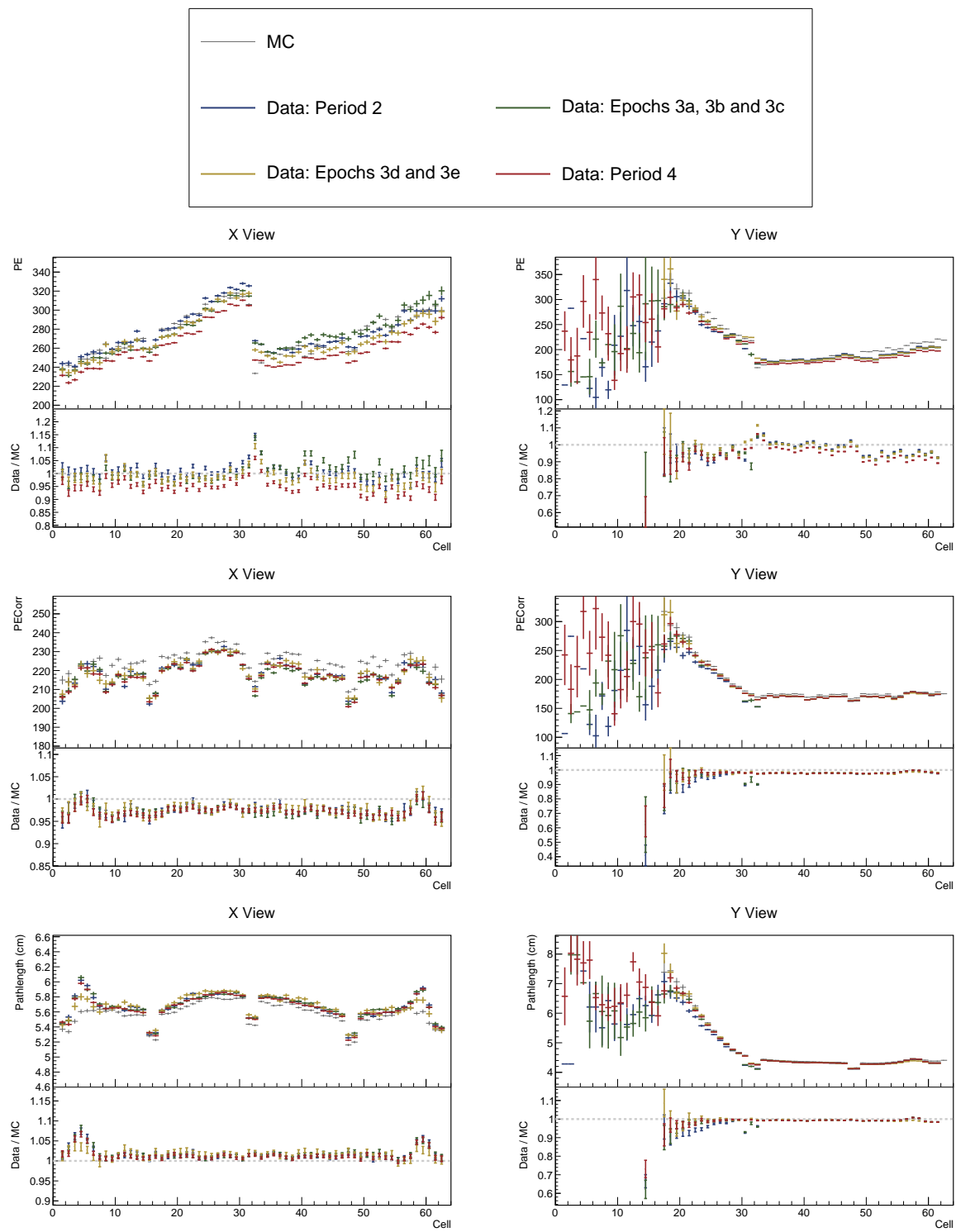


Figure 44: ...

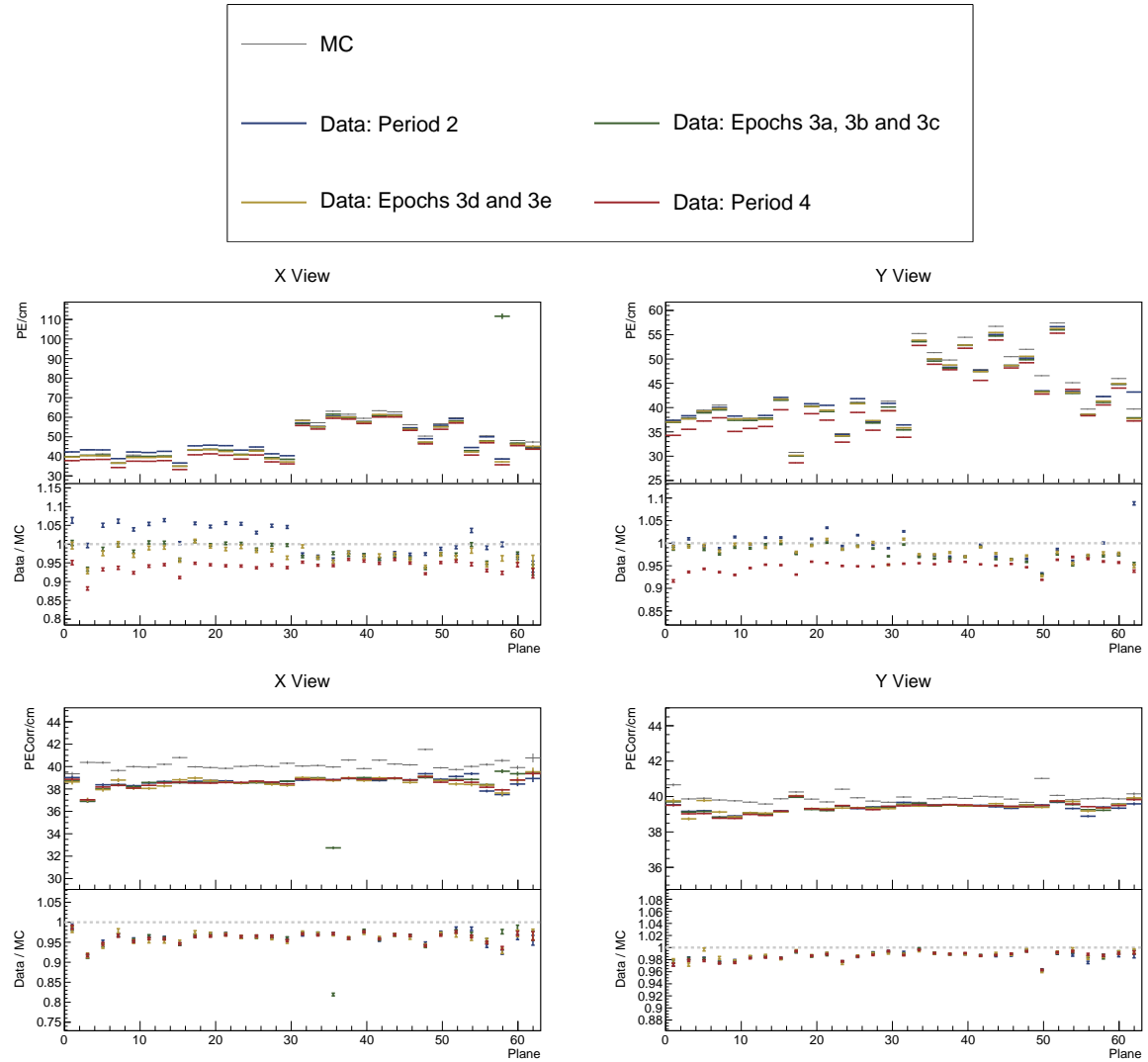


Figure 45: ...

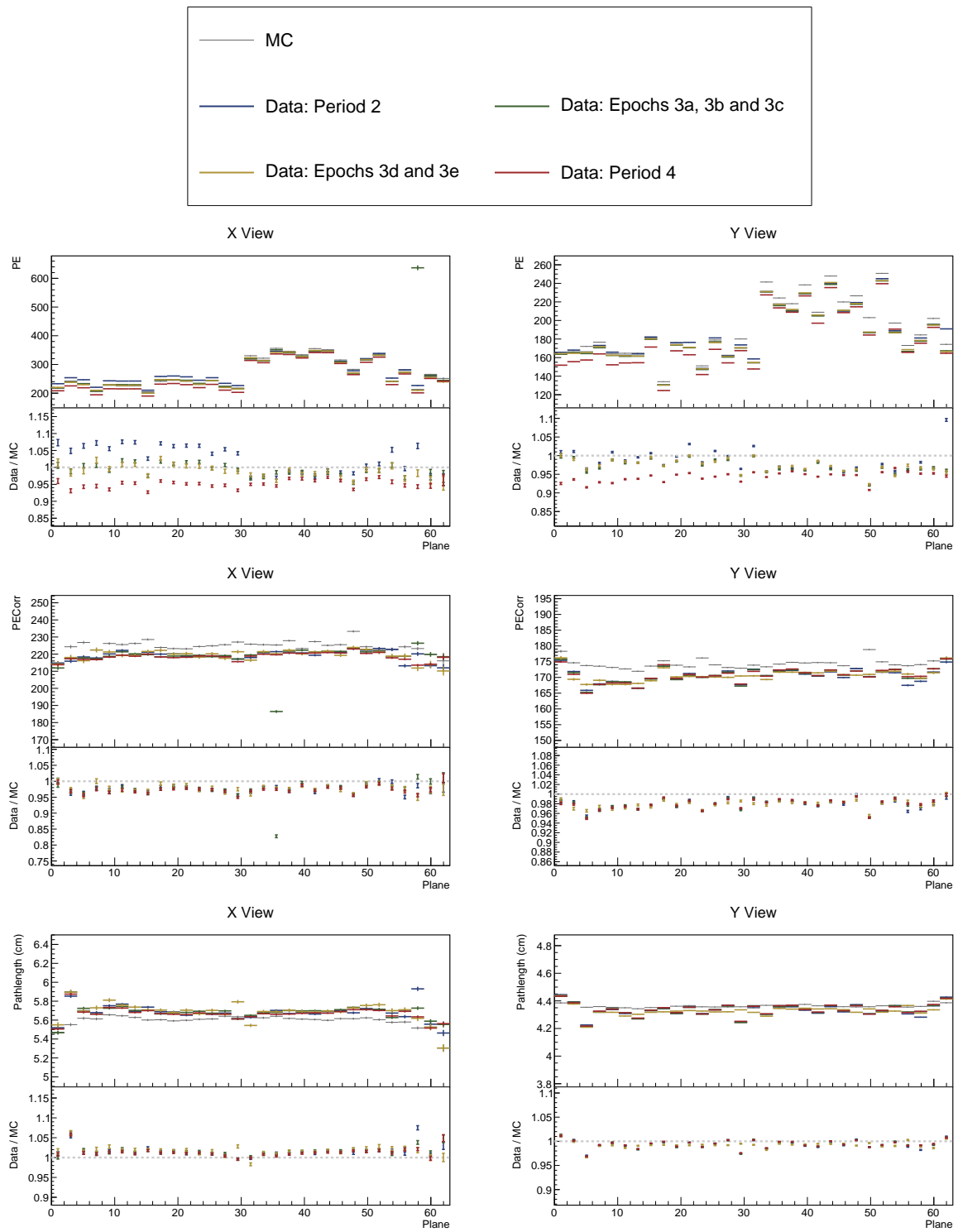


Figure 46: ...

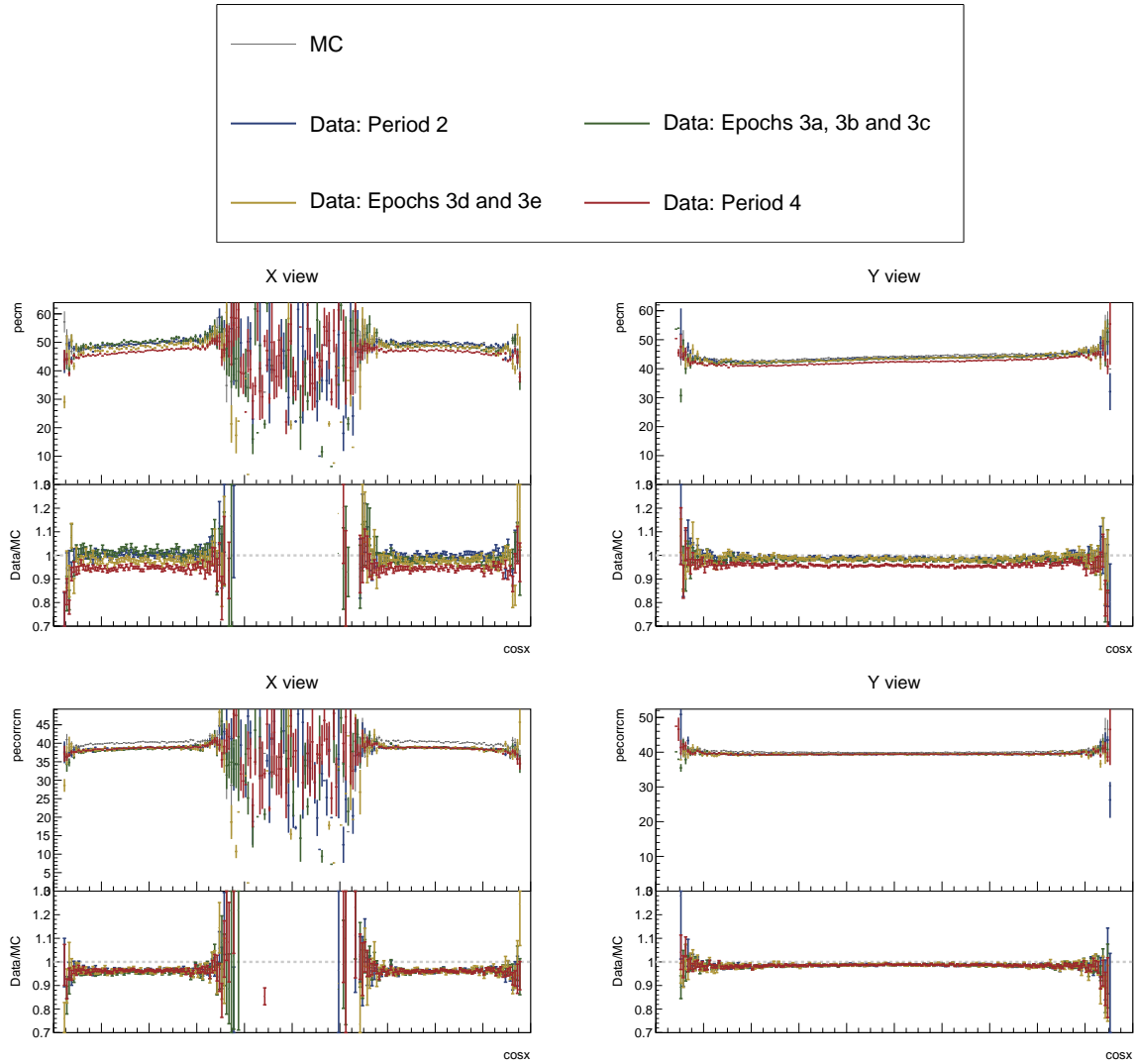


Figure 47: ...

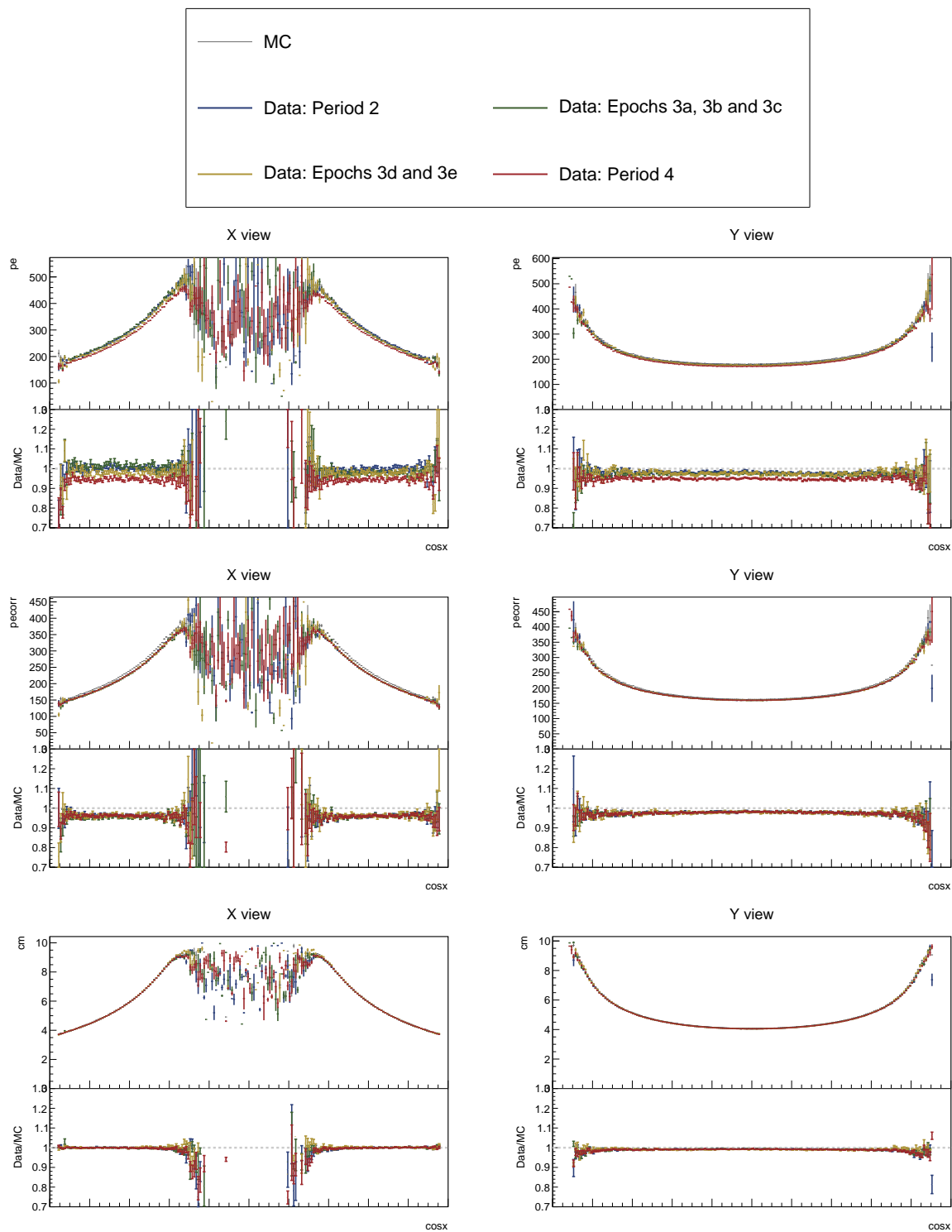


Figure 48: ...

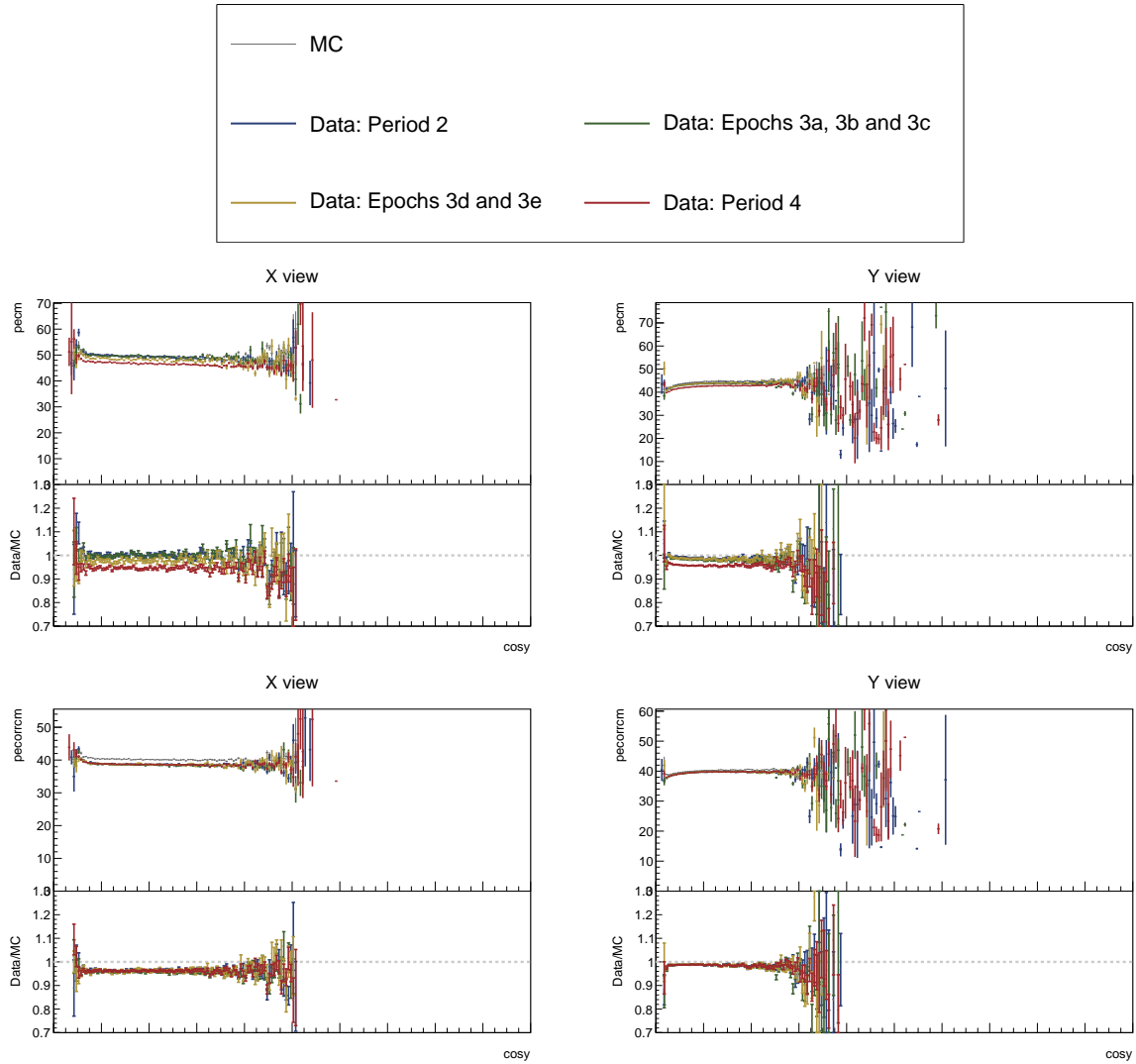


Figure 49: ...

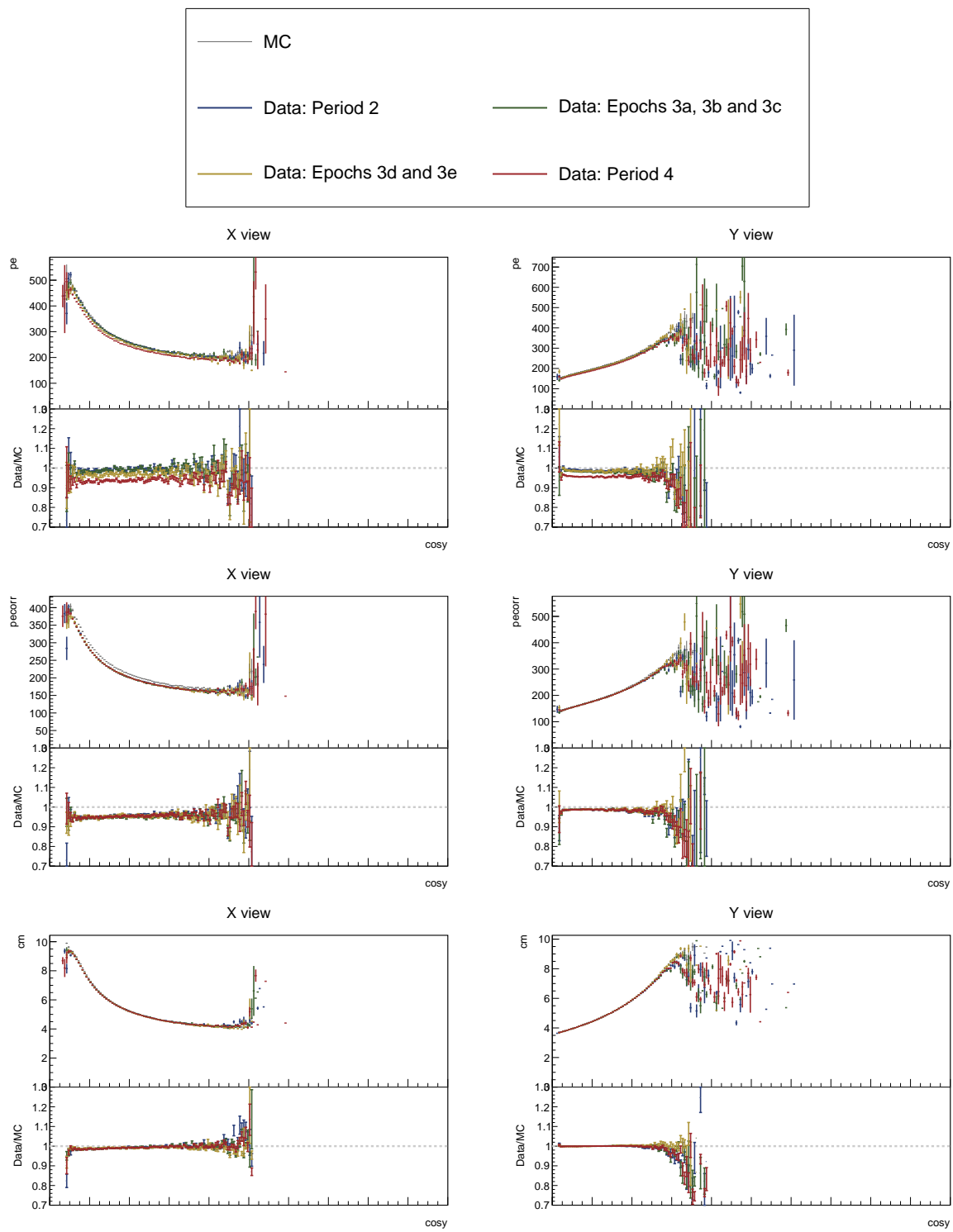


Figure 50: ...

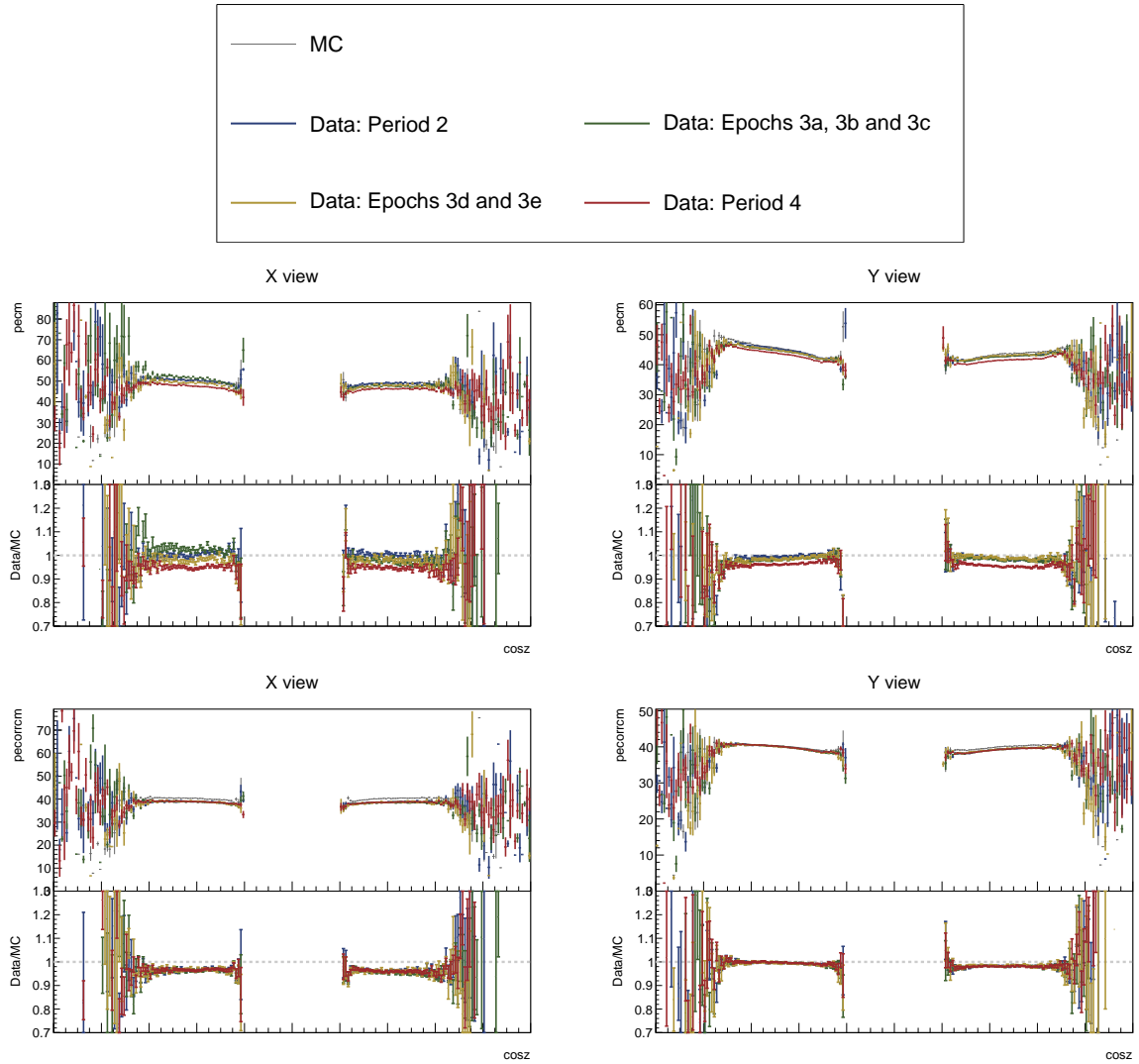


Figure 51: ...

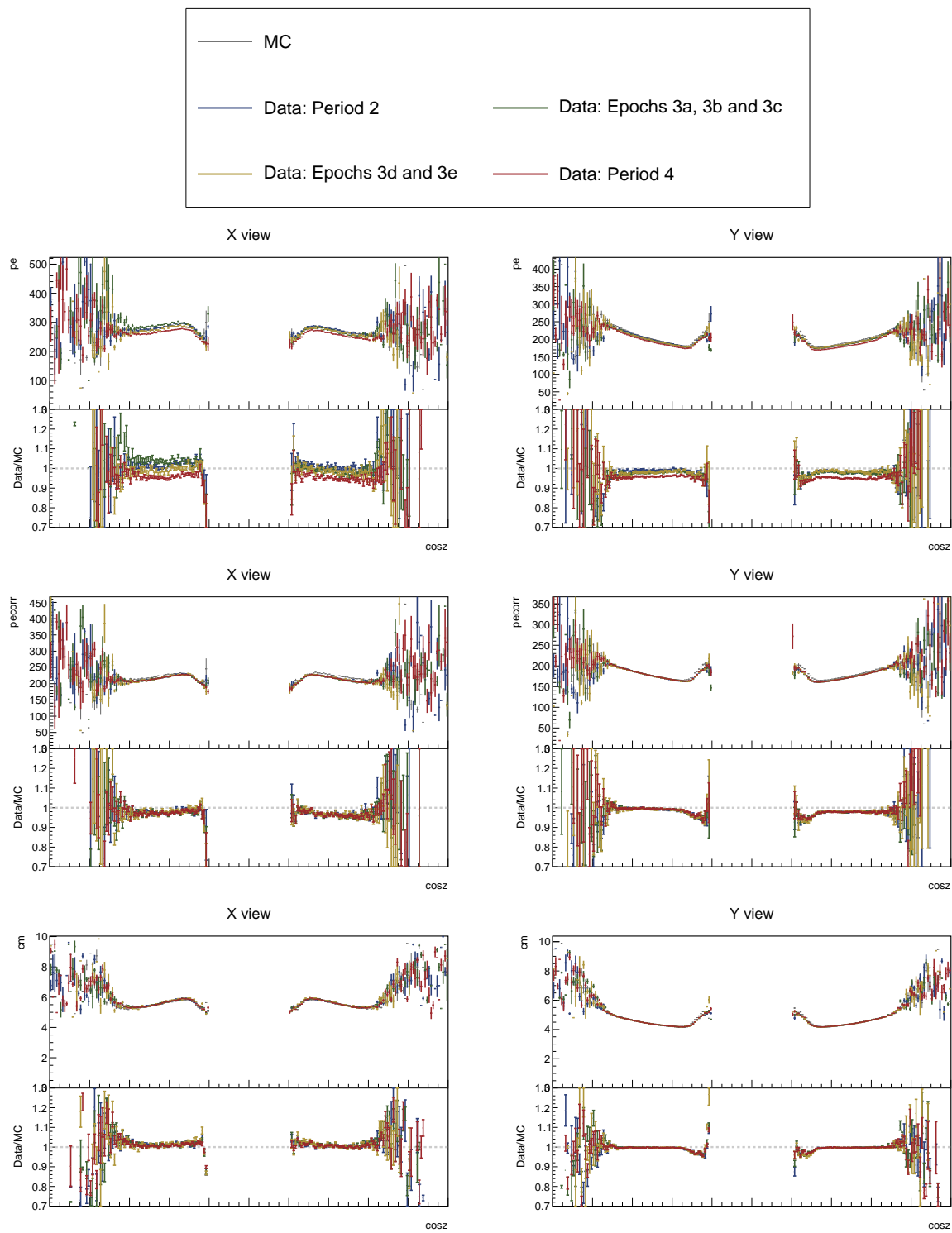


Figure 52: ...

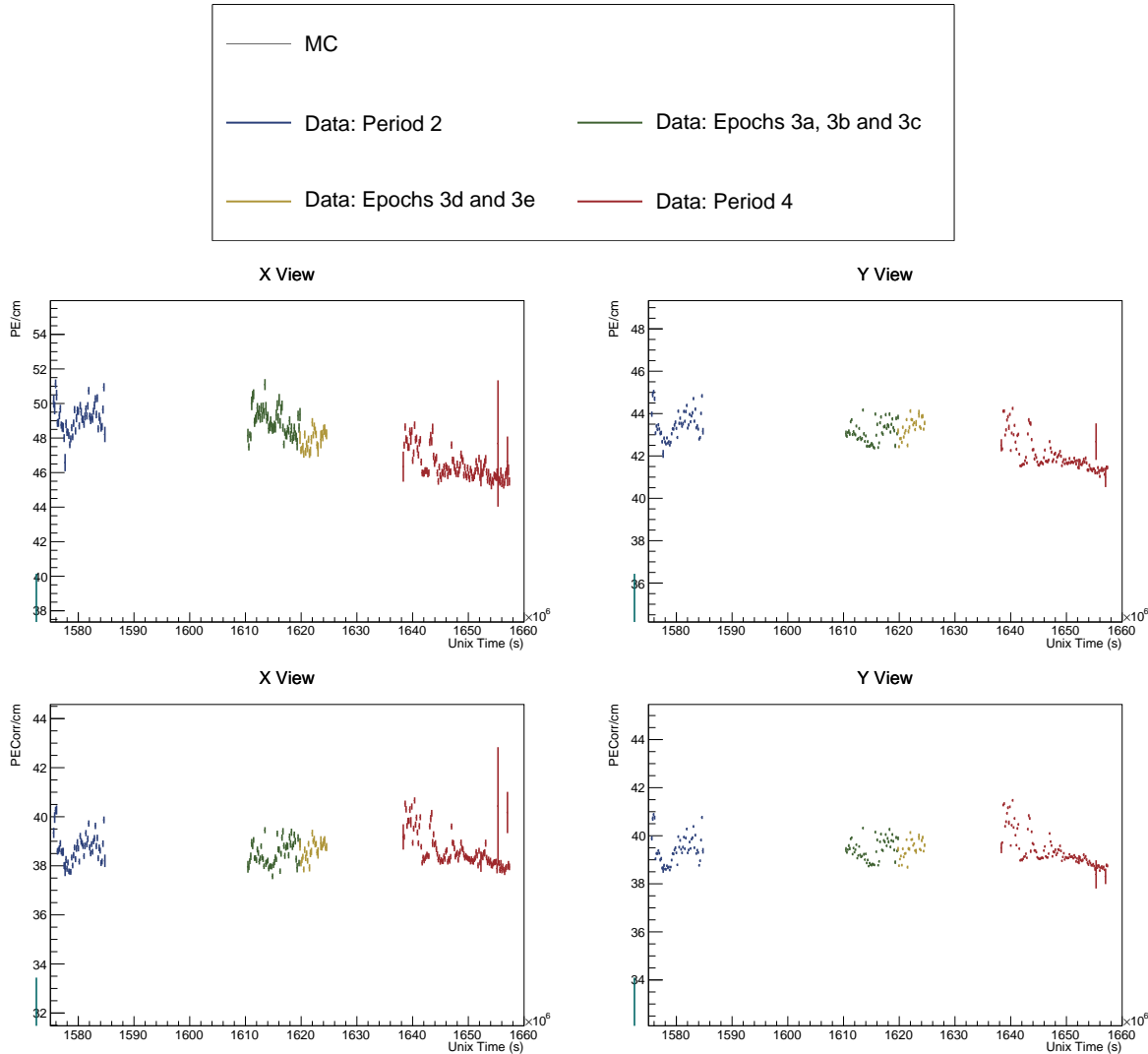


Figure 53: ...

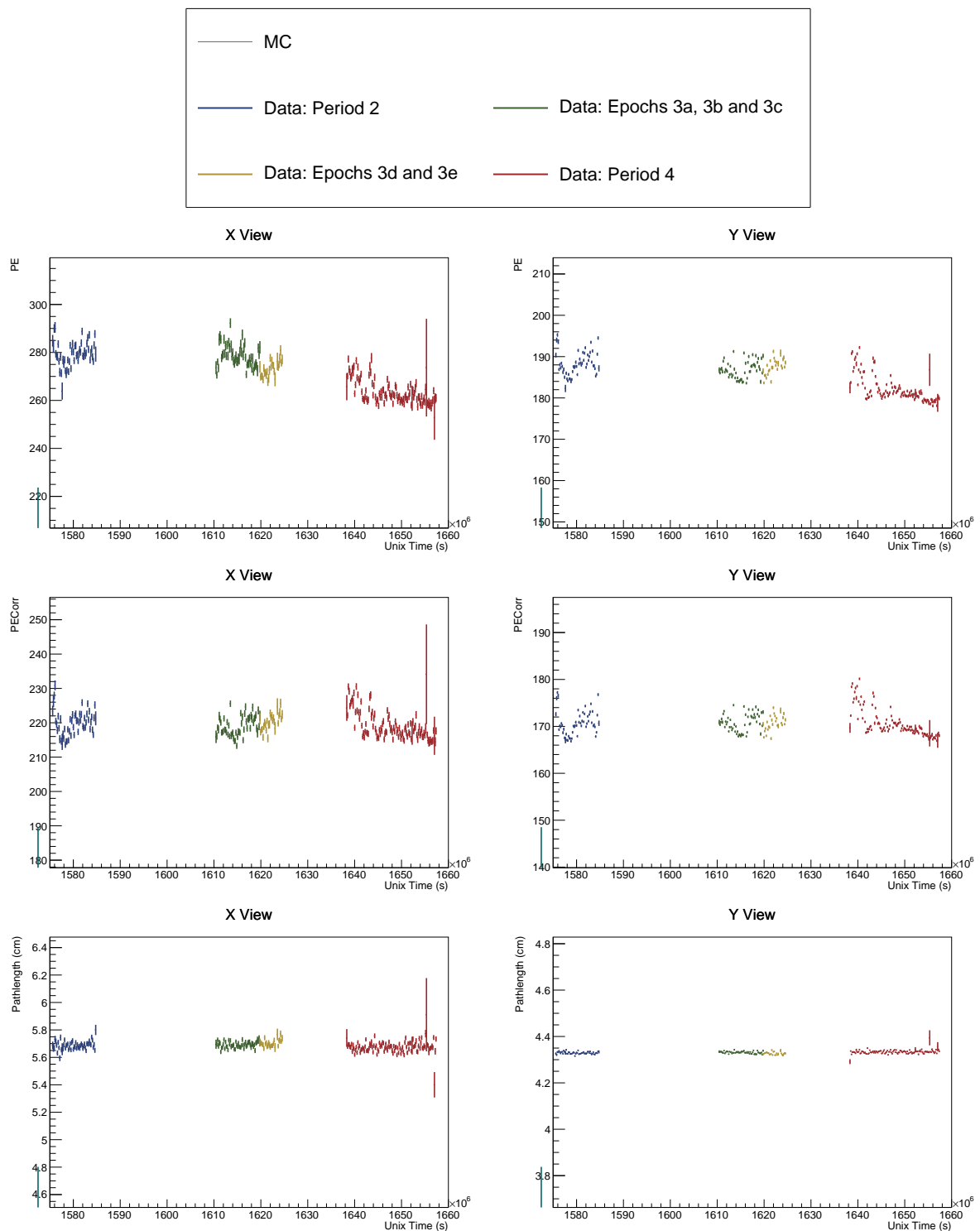


Figure 54: ...

459 **5 Conclusion**

460 TO DO: Write a conclusion

461 **References**

- 462 [1] Alex Sousa. Test Beam Plenary Update - FNAL September 2018. NOVA Document  
463 33012, September 2018. NOvA internal document. URL: <https://nova-docdb.fnal.gov/cgi-bin/sso>ShowDocument?docid=33012>.
- 465 [2] Alex Sousa, Ryan Nichol, Karol Lang, and Jeff Nelson. NOvA Test Beam Task Force  
466 Report. NOVA Document 15750, August 2016. NOvA technical note. URL: <https://nova-docdb.fnal.gov/cgi-bin/sso>ShowDocument?docid=15750>.
- 468 [3] Kevin Mulder. TB Calibration update. NOVA Document 42700, January 2020.  
469 NOvA internal document. URL: <https://nova-docdb.fnal.gov/cgi-bin/sso>ShowDocument?docid=42700>.
- 471 [4] Anna Maureen Hall. TB P2 Calib Update. NOVA Document 50786, June 2021.  
472 NOvA internal document. URL: <https://nova-docdb.fnal.gov/cgi-bin/sso>ShowDocument?docid=50786>.
- 474 [5] Robert Kralik. Test Beam calibration results - Spring 2023. NOVA Document 59024, June  
475 2023. NOvA internal document. URL: <https://nova-docdb.fnal.gov/cgi-bin/sso>ShowDocument?docid=59024>.
- 477 [6] Alex Sousa. NOvA Test Beam Status and Plans - Support Documentation. NOVA Doc-  
478 ument 22172-v2, October 2017. NOvA technical note. URL: <https://nova-docdb.fnal.gov/cgi-bin/sso>ShowDocument?docid=22172>.
- 480 [7] Alex Sousa. NOvA Test Beam Plenary @ IU Collaboration Meeting. NOVA Document  
481 29543, May 2018. NOvA internal document. URL: <https://nova-docdb.fnal.gov/cgi-bin/sso>ShowDocument?docid=29543>.
- 483 [8] Michael Wallbank. Final Test Beam Updates (Geometry and Other!). NOVA Document  
484 58388, April 2023. NOvA internal document. URL: <https://nova-docdb.fnal.gov/cgi-bin/sso>ShowDocument?docid=58388>.
- 486 [9] Michael Wallbank. Understanding, Improving, Validating the Test Beam Geometry.  
487 NOVA Document 57955, February 2023. NOvA internal document. URL: <https://nova-docdb.fnal.gov/cgi-bin/sso>ShowDocument?docid=57955>.
- 489 [10] Robert Kralik. Test beam calibration update. NOVA Document 57516-v2, January  
490 2023. NOvA internal document. URL: <https://nova-docdb.fnal.gov/cgi-bin/sso>ShowDocument?docid=57516>.
- 492 [11] Alex Sousa. Test Beam Plenary Update - Jun. 6, 2019. NOVA Document 38349, June  
493 2019. NOvA internal document. URL: <https://nova-docdb.fnal.gov/cgi-bin/sso>ShowDocument?docid=38349>.

- 495 [12] Alex Sousa. Filling System and Scintillator Status. NOVA Document 34067, November  
496 2018. NOvA internal document. URL: <https://nova-docdb.fnal.gov/cgi-bin/sso>ShowDocument?docid=34067>.
- 498 [13] Junting Huang, Will Flanagan, and Beatriz Tapia Oregui. Test Beam: Light Yield of  
499 the Liquid Scintillator Drained from the NDOS Detector. NOVA Document 38740, July  
500 2019. NOvA internal document. URL: <https://nova-docdb.fnal.gov/cgi-bin/sso>ShowDocument?docid=38740>.
- 502 [14] Dung Phan. Test Beam: Tintometer Measurement of Texas A&M oil. NOVA Document  
503 39088, July 2019. NOvA internal document. URL: <https://nova-docdb.fnal.gov/cgi-bin/sso>ShowDocument?docid=39088>.
- 505 [15] Alex Sousa. Test Beam Scintillator Fill Plan. NOVA Document 34196, November  
506 2018. NOvA internal document. URL: <https://nova-docdb.fnal.gov/cgi-bin/sso>ShowDocument?docid=34196>.
- 508 [16] Alex Sousa. 2nd Block Filling Status - Nov. 18, 2019. NOVA Document 41961, November  
509 2019. NOvA internal document. URL: <https://nova-docdb.fnal.gov/cgi-bin/sso>ShowDocument?docid=41961>.
- 511 [17] Teresa Megan Lackey. *Proton Scattering in NOvA Test Beam*. PhD thesis, Indiana U.,  
512 July 2022.
- 513 [18] David Northacker, Alex Sousa, and Yagmur Torun. Test Beam - Overfilling Horizontal  
514 Planes. NOVA Document 49439, March 2021. NOvA internal document. URL: <https://nova-docdb.fnal.gov/cgi-bin/sso>ShowDocument?docid=49439>.
- 516 [19] Keith Matera et al. Calibration Technotes. NOVA Document 13579, January  
517 2017. NOvA technical note. URL: <https://nova-docdb.fnal.gov/cgi-bin/sso>ShowDocument?docid=13579>.
- 519 [20] Christopher J. Backhouse. Cell-by-cell attenuation calibration of the NOvA detectors.  
520 NOVA Document 7410, December 2014. NOvA technical note. URL: <https://nova-docdb.fnal.gov/cgi-bin/sso>ShowDocument?docid=7410>.
- 522 [21] Evan David Niner. *Observation of Electron Neutrino Appearance in the NuMI Beam with  
523 the NOvA Experiment*. PhD thesis, Indiana U., 2015. doi:10.2172/1221353.
- 524 [22] Christopher J. Backhouse. Timing bias introduced by incorrect interpretation of the  
525 nanoslice. NOVA Document 13518, June 2015. NOvA technical note. URL: <https://nova-docdb.fnal.gov/cgi-bin/sso>ShowDocument?docid=13518>.
- 527 [23] Luke Vinton. Calorimetric Energy Scale Calibration of the NOvA Detectors. NOVA Doc-  
528 ument 13579, document FA\_Calorimetric\_energy\_scale.pdf, July 2015. NOvA technical  
529 note. URL: <https://nova-docdb.fnal.gov/cgi-bin/sso>ShowDocument?docid=13579>.
- 531 [24] Keith Matera. Keith's Swell Guide: The Calibration Meta. NOVA Document 13579, doc-  
532 ument Calibration\_Meta\_READFIRST.pdf, January 2017. NOvA technical note. URL:  
533 <https://nova-docdb.fnal.gov/cgi-bin/sso>ShowDocument?docid=13579>.

- 534 [25] Christopher Backhouse, Alexender Radovic, and Prabhjot Singh. The Attenuation and  
535 Threshold Calibration of the NOvA detectors. NOVA Document 13579, document  
536 SA\_Attenuation\_and\_Threshold.pdf, May 2016. NOvA technical note. URL: <https://nova-docdb.fnal.gov/cgi-bin/sso>ShowDocument?docid=13579>.
- 537
- 538 [26] Ryan J. Nichol. Fibre brightness from cosmic muon data. NOVA Document 34909, De-  
539 cember 2018. NOvA technical note. URL: <https://nova-docdb.fnal.gov/cgi-bin/sso>ShowDocument?docid=34909>.
- 540
- 541 [27] Robert Kralik. The Attenuation and Threshold Calibration of the NOvA detectors. NOVA  
542 Document 60026, October 2023. NOvA technical note. URL: <https://nova-docdb.fnal.gov/cgi-bin/sso>ShowDocument?docid=60026>.
- 543
- 544 [28] Anna Maureen Hall. TB P2 Calib. Summary. NOVA Document 49674, March 2021.  
545 NOvA internal document. URL: <https://nova-docdb.fnal.gov/cgi-bin/sso>ShowDocument?docid=49674>.
- 546
- 547 [29] Matthew Strait. Update on light level tuning. NOVA Document 43249, February  
548 2020. NOvA internal document. URL: <https://nova-docdb.fnal.gov/cgi-bin/sso>ShowDocument?docid=43249>.
- 549